FRAMATOME COGEMA FUELS

October 30, 2000
GR00-166.doc

U. S. Nuclear Regulatory Commission
ATTN: Document Control Desk
Washington, DC 20555

Subject: Submittal of Topical Report BAW-10133P, Rev. 1, Addendum 1 and Addendum 2, "Mark-C Fuel Assembly LOCA-Seismic Analysis," October 2000.

Gentlemen:

Enclosed are fifteen (15) copies of Topical Report BAW-10133P-A, Rev. 1, Addendum 1 and Addendum 2 and twelve (12) copies of Topical Report BAW-10133-A, Rev. 1, Addendum 1 and Addendum 2. These reports will serve as the accepted versions, proprietary and non-proprietary of BAW-10133P-A, Rev. 1, Addendum 1 and Addendum 2 which was recently reviewed and found to be acceptable by the NRC staff. This report provides the faulted condition methodology that FCF is using in LOCA-seismic structural evaluations.

Copies of the NRC acceptance letter and accompanying SER are included between the title page and the table of contents of Addendum 1 of the report. Copies of responses to the NRC requests for additional information are included as Appendix C of Addendum 1 and Appendix A of Addendum 2.

In accordance with 10 CFR 2.790, FCF requests that BAW-10133P-A, Rev. 1, Addendum 1 and Addendum 2 be considered proprietary and withheld from public disclosure. An affidavit supporting this request is attached.

Very truly yours,

T A Coleman

T. A. Coleman, Vice President
Government Relations

cc: J. S. Wermiel, NRC
S. L. Wu, NRC
S. N. Bailey, NRC
M. A. Schoppman
R. N. Edwards
C. E. Beyer, PNL
20A13 File/Records Management

T008
1/12
Non Prop
Enc

FRAMATOME TECHNOLOGIES

Framatome Cogema Fuels
P.O. Box 11646, Lynchburg, VA 24506-1646
Telephone: 804-832-5000 Fax: 804-832-5167

bcc: J. B. Andrews
G. A. Meyer
A. B. Copsey
M. E. Aldrich
C. F. McPhatter
R. D. Williamson
L. W. Newman
S. J. Shah
G. T. Williams

AFFIDAVIT OF THOMAS A. COLEMAN

A. My name is Thomas A. Coleman. I am Vice President of Government Relations for Framatome Cogema Fuels (FCF). Therefore, I am authorized to execute this Affidavit.

B. I am familiar with the criteria applied by FCF to determine whether certain information of FCF is proprietary and I am familiar with the procedures established within FCF to ensure the proper application of these criteria.

C. In determining whether an FCF document is to be classified as proprietary information, an initial determination is made by the Unit Manager, who is responsible for originating the document, as to whether it falls within the criteria set forth in Paragraph D hereof. If the information falls within any one of these criteria, it is classified as proprietary by the originating Unit Manager. This initial determination is reviewed by the cognizant Section Manager. If the document is designated as proprietary, it is reviewed again by personnel and other management within FCF as designated by the Vice President of Government Relations to assure that the regulatory requirements of 10 CFR Section 2.790 are met.

D. The following information is provided to demonstrate that the provisions of 10 CFR Section 2.790 of the Commission's regulations have been considered:

(i) The information has been held in confidence by FCF. Copies of the document are clearly identified as proprietary. In addition, whenever FCF transmits the information to a customer, customer's agent, potential customer or regulatory agency, the transmittal requests the recipient to hold the information as proprietary. Also, in order to strictly limit any potential or actual customer's use of proprietary information, the substance of the following provision is included in all agreements entered into by FCF, and an equivalent version of the proprietary provision is included in all of FCF's proposals:

"Any proprietary information concerning Company's or its Supplier's products or manufacturing processes which is so designated by Company or its Suppliers and disclosed to Purchaser incident to the performance of such contract shall remain the property of Company or its Suppliers and is disclosed in confidence, and Purchaser shall not publish or otherwise disclose it to others without the written approval of Company, and no rights, implied or otherwise, are granted to produce or have produced any products or to practice or cause to be practiced any manufacturing processes covered thereby.

Notwithstanding the above, Purchaser may provide the NRC or any other regulatory agency with any such proprietary information as the NRC or such other agency may require; provided, however, that Purchaser shall first give Company written notice of such proposed disclosure and Company shall have the right to amend such proprietary information so as to make it non-proprietary. In the event that Company cannot amend such proprietary information, Purchaser shall, prior to disclosing such information, use its best efforts to obtain a commitment from NRC or such other agency to have such information withheld from public inspection.

Company shall be given the right to participate in pursuit of such confidential treatment."

(ii) The following criteria are customarily applied by FCF in a rational decision process to determine whether the information should be classified as proprietary. Information may be classified as proprietary if one or more of the following criteria are met:

a. Information reveals cost or price information, commercial strategies, production capabilities, or budget levels of FCF, its customers or suppliers.

b. The information reveals data or material concerning FCF research or development plans or programs of present or potential competitive advantage to FCF.

c. The use of the information by a competitor would decrease his expenditures, in time or resources, in designing, producing or marketing a similar product.

d. The information consists of test data or other similar data concerning a process, method or component, the application of which results in a competitive advantage to FCF.

e. The information reveals special aspects of a process, method, component or the like, the exclusive use of which results in a competitive advantage to FCF.

f. The information contains ideas for which patent protection may be sought.

The document(s) listed on Exhibit "A", which is attached hereto and made a part hereof, has been evaluated in accordance with normal FCF procedures with respect to classification and has been found to contain information which falls within one or more of the criteria enumerated above. Exhibit "B", which is attached hereto and made a part hereof, specifically identifies the criteria applicable to the document(s) listed in Exhibit "A".

(iii) The document(s) listed in Exhibit "A", which has been made available to the United States Nuclear Regulatory Commission was made available in confidence with a request that the document(s) and the information contained therein be withheld from public disclosure.

(iv) The information is not available in the open literature and to the best of our knowledge is not known by Combustion Engineering, Siemens, General Electric, Westinghouse or other current or potential domestic or foreign competitors of Framatome Cogema Fuels.

(v) Specific information with regard to whether public disclosure of the information is likely to cause harm to the competitive position of FCF, taking into account the value of the information to FCF; the amount of effort or money expended by FCF developing the information; and the ease or difficulty with which the information could be properly duplicated by others is given in Exhibit "B".

E. I have personally reviewed the document(s) listed on Exhibit "A" and have found that it is considered proprietary by FCF because it contains information which falls within one or more of the criteria enumerated in Paragraph D, and it is information which is customarily held in confidence and protected as proprietary information by FCF. This report comprises information utilized by FCF in its business which afford FCF an opportunity to obtain a

competitive advantage over those who may wish to know or use the information contained in the document(s).

TAColeman

THOMAS A. COLEMAN

State of Virginia)
) SS. Lynchburg
City of Lynchburg)

Thomas A. Coleman, being duly sworn, on his oath deposes and says that he is the person who subscribed his name to the foregoing statement, and that the matters and facts set forth in the statement are true.

TAColeman

THOMAS A. COLEMAN

Subscribed and sworn before me
this 30th day of October 2000.

Wanda L. Wade
Notary Public in and for the City
of Lynchburg, State of Virginia.

My Commission Expires 8/31/01

EXHIBITS A & B

EXHIBIT A

BAW-10133P, Rev. 1, Addendum 1 and Addendum 2, "Mark-C Fuel Assembly LOCA-Seismic Analysis."

EXHIBIT B

The above listed document contains information which is considered Proprietary in accordance with Criteria b, c, and d of the attached affidavit.

BAW-10133-A, Rev. 1
Addendum 1 and Addendum 2
October 2000

ADDENDUM 1 AND ADDENDUM 2 TO BAW-10133-A, REV. 1 MARK-C FUEL ASSEMBLY LOCA-SEISMIC ANALYSES

FRAMATOME COGEMA FUELS

FRAMATOME COGEMA FUELS

October 30, 2000
GR00-166.doc

U. S. Nuclear Regulatory Commission
ATTN: Document Control Desk
Washington, DC 20555

Subject: Submittal of Topical Report BAW-10133P, Rev. 1, Addendum 1 and Addendum 2, "Mark-C Fuel Assembly LOCA-Seismic Analysis," October 2000.

Gentlemen:

Enclosed are fifteen (15) copies of Topical Report BAW-10133P-A, Rev. 1, Addendum 1 and Addendum 2 and twelve (12) copies of Topical Report BAW-10133-A, Rev. 1, Addendum 1 and Addendum 2. These reports will serve as the accepted versions, proprietary and non-proprietary of BAW-10133P-A, Rev. 1, Addendum 1 and Addendum 2 which was recently reviewed and found to be acceptable by the NRC staff. This report provides the faulted condition methodology that FCF is using in LOCA-seismic structural evaluations.

Copies of the NRC acceptance letter and accompanying SER are included between the title page and the table of contents of Addendum 1 of the report. Copies of responses to the NRC requests for additional information are included as Appendix C of Addendum 1 and Appendix A of Addendum 2.

In accordance with 10 CFR 2.790, FCF requests that BAW-10133P-A, Rev. 1, Addendum 1 and Addendum 2 be considered proprietary and withheld from public disclosure. An affidavit supporting this request is attached.

Very truly yours,

T A Coleman

T. A. Coleman, Vice President
Government Relations

cc: J. S. Wermiel, NRC
S. L. Wu, NRC
S. N. Bailey, NRC
M. A. Schoppman
R. N. Edwards
C. E. Beyer, PNL
20A13 File/Records Management

FRAMATOME TECHNOLOGIES

Framatome Cogema Fuels
P.O. Box 11646, Lynchburg, VA 24506-1646
Telephone: 804-832-5000 Fax: 804-832-5167

AFFIDAVIT OF THOMAS A. COLEMAN

A. My name is Thomas A. Coleman. I am Vice President of Government Relations for Framatome Cogema Fuels (FCF). Therefore, I am authorized to execute this Affidavit.

B. I am familiar with the criteria applied by FCF to determine whether certain information of FCF is proprietary and I am familiar with the procedures established within FCF to ensure the proper application of these criteria.

C. In determining whether an FCF document is to be classified as proprietary information, an initial determination is made by the Unit Manager, who is responsible for originating the document, as to whether it falls within the criteria set forth in Paragraph D hereof. If the information falls within any one of these criteria, it is classified as proprietary by the originating Unit Manager. This initial determination is reviewed by the cognizant Section Manager. If the document is designated as proprietary, it is reviewed again by personnel and other management within FCF as designated by the Vice President of Government Relations to assure that the regulatory requirements of 10 CFR Section 2.790 are met.

D. The following information is provided to demonstrate that the provisions of 10 CFR Section 2.790 of the Commission's regulations have been considered:

(i) The information has been held in confidence by FCF. Copies of the document are clearly identified as proprietary. In addition, whenever FCF transmits the information to a customer, customer's agent, potential customer or regulatory agency, the transmittal requests the recipient to hold the information as proprietary. Also, in order to strictly limit any potential or actual customer's use of proprietary information, the substance of the following provision is included in all agreements entered into by FCF, and an equivalent version of the proprietary provision is included in all of FCF's proposals:

"Any proprietary information concerning Company's or its Supplier's products or manufacturing processes which is so designated by Company or its Suppliers and disclosed to Purchaser incident to the performance of such contract shall remain the property of Company or its Suppliers and is disclosed in confidence, and Purchaser shall not publish or otherwise disclose it to others without the written approval of Company, and no rights, implied or otherwise, are granted to produce or have produced any products or to practice or cause to be practiced any manufacturing processes covered thereby.

Notwithstanding the above, Purchaser may provide the NRC or any other regulatory agency with any such proprietary information as the NRC or such other agency may require; provided, however, that Purchaser shall first give Company written notice of such proposed disclosure and Company shall have the right to amend such proprietary information so as to make it non-proprietary. In the event that Company cannot amend such proprietary information, Purchaser shall, prior to disclosing such information, use its best efforts to obtain a commitment from NRC or such other agency to have such information withheld from public inspection.

Company shall be given the right to participate in pursuit of such confidential treatment."

(ii) The following criteria are customarily applied by FCF in a rational decision process to determine whether the information should be classified as proprietary. Information may be classified as proprietary if one or more of the following criteria are met:

a. Information reveals cost or price information, commercial strategies, production capabilities, or budget levels of FCF, its customers or suppliers.

b. The information reveals data or material concerning FCF research or development plans or programs of present or potential competitive advantage to FCF.

c. The use of the information by a competitor would decrease his expenditures, in time or resources, in designing, producing or marketing a similar product.

d. The information consists of test data or other similar data concerning a process, method or component, the application of which results in a competitive advantage to FCF.

e. The information reveals special aspects of a process, method, component or the like, the exclusive use of which results in a competitive advantage to FCF.

f. The information contains ideas for which patent protection may be sought.

The document(s) listed on Exhibit "A", which is attached hereto and made a part hereof, has been evaluated in accordance with normal FCF procedures with respect to classification and has been found to contain information which falls within one or more of the criteria enumerated above. Exhibit "B", which is attached hereto and made a part hereof, specifically identifies the criteria applicable to the document(s) listed in Exhibit "A".

(iii) The document(s) listed in Exhibit "A", which has been made available to the United States Nuclear Regulatory Commission was made available in confidence with a request that the document(s) and the information contained therein be withheld from public disclosure.

(iv) The information is not available in the open literature and to the best of our knowledge is not known by Combustion Engineering, Siemens, General Electric, Westinghouse or other current or potential domestic or foreign competitors of Framatome Cogema Fuels.

(v) Specific information with regard to whether public disclosure of the information is likely to cause harm to the competitive position of FCF, taking into account the value of the information to FCF; the amount of effort or money expended by FCF developing the information; and the ease or difficulty with which the information could be properly duplicated by others is given in Exhibit "B".

E. I have personally reviewed the document(s) listed on Exhibit "A" and have found that it is considered proprietary by FCF because it contains information which falls within one or more of the criteria enumerated in Paragraph D, and it is information which is customarily held in confidence and protected as proprietary information by FCF. This report comprises information utilized by FCF in its business which afford FCF an opportunity to obtain a

competitive advantage over those who may wish to know or use the information contained in the document(s).

T A Coleman

THOMAS A. COLEMAN

State of Virginia)
) SS. Lynchburg
City of Lynchburg)

Thomas A. Coleman, being duly sworn, on his oath deposes and says that he is the person who subscribed his name to the foregoing statement, and that the matters and facts set forth in the statement are true.

T A Coleman

THOMAS A. COLEMAN

Subscribed and sworn before me
this 30th day of October 2000.

Wanda L. Wade
Notary Public in and for the City
of Lynchburg, State of Virginia.

My Commission Expires 8/31/01

EXHIBITS A & B

EXHIBIT A

BAW-10133P, Rev. 1, Addendum 1 and Addendum 2, "Mark-C Fuel Assembly LOCA-Seismic Analysis."

EXHIBIT B

The above listed document contains information which is considered Proprietary in accordance with Criteria b, c, and d of the attached affidavit.

ADDENDUM 1 TO BAW-10133-A, Rev.1
Mark-C Fuel Assembly
LOCA-Seismic Analyses

Framatome Cogema Fuels
P.O. Box 10935
3315 Old Forest Drive
Lynchburg, Va. 24506-0935

UNITED STATES
NUCLEAR REGULATORY COMMISSION
WASHINGTON, D.C. 20555-0001

October 17, 2000

Mr. T. A. Coleman, Vice President
Government Relations
Framatome Cogema Fuels
3315 Old Forest Road
P.O. Box 10935
Lynchburg, VA 24506-3663

SUBJECT: ACCEPTANCE FOR REFERENCING OF LICENSING TOPICAL REPORT BAW-10133P, REVISION 1, ADDENDA 1 AND 2, "MARK-C FUEL ASSEMBLY LOCA-SEISMIC ANALYSES" (TAC NOS. M99906 AND MA5902)

Dear Mr. Coleman:

The U.S. Nuclear Regulatory Commission (NRC) staff has completed its review of the subject topical report addenda, which were submitted by Framatome Cogema Fuels (FCF) by letters dated September 30, 1997, and May 5, 1999. The staff has found that the addenda are acceptable for referencing in licensing applications to the extent specified and under the limitations delineated in the report addenda and the associated NRC safety evaluation, which is enclosed. The safety evaluation defines the basis for the acceptance of the report addenda. The staff will not repeat its review of the matters described in BAW-10133P, Revision 1, Addenda 1 and 2, when they appear as a reference in license applications, except to ensure that the material presented applies to the specific plant involved.

In accordance with procedures established in NUREG-0390, the NRC requests that FCF publish accepted versions of the submittals, proprietary and non-proprietary, within three months of receipt of this letter. The accepted versions shall incorporate this letter and the enclosed safety evaluation between the title page and the abstract, and an -A (designating accepted) following the report identification symbol. The accepted version shall also incorporate all communications between FCF and the NRC during this review.

Pursuant to 10 CFR 2.790, the staff has determined that the enclosed safety evaluation does not contain proprietary information. However, the staff will delay placing the safety evaluation in the public document room for 10 calendar days from the date of this letter to allow you the opportunity to comment on the proprietary aspects only. If, after that time, you do not request that all or portions of the safety evaluation be withheld from public disclosure in accordance with 10 CFR 2.790, the safety evaluation will be placed in the NRC Public Document Room.

Should our acceptance criteria or regulations change so that our conclusions as to the acceptability of the report are no longer valid, applicants referencing the topical report will be expected to revise and resubmit its respective documentation, or submit justification for the continued applicability of the topical report without revision of the respective documentation.

Should you have any questions or wish further clarification, please call Stewart Bailey at (301) 415-1321.

Sincerely,

Stuart A. Richards, Director
Project Directorate IV & Decommissioning
Division of Licensing Project Management
Office of Nuclear Reactor Regulation

Project No. 693

Enclosure: Safety Evaluation

cc w/encl:
Mr. F. McPhatter, Manager
Framatome Cogema Fuels
3315 Old Forest Road
P.O. Box 10935
Lynchburg, VA 24506-0935

Mr. Michael Schoppman
Licensing Manager
Framatome Technologies, Inc.
1700 Rockville Pike, Suite 525
Rockville, MD 20852-1631

UNITED STATES
NUCLEAR REGULATORY COMMISSION
WASHINGTON, D.C. 20555-0001

SAFETY EVALUATION BY THE OFFICE OF NUCLEAR REACTOR REGULATION

TOPICAL REPORT BAW-10133P, REVISION 1, ADDENDA 1 AND 2

"MARK-C FUEL ASSEMBLY LOCA-SEISMIC ANALYSES"

FRAMATOME COGEMA FUELS

PROJECT NO. 693

1.0 INTRODUCTION

By letters dated September 30, 1997, and May 5, 1999 (References 1 and 2), Framatome Cogema Fuels (FCF) submitted Addendum 1 and Addendum 2, respectively, to Topical Report BAW-10133P, "Mark-C Fuel Assembly LOCA-Seismic Analyses," Revision 1, for the U.S. Nuclear Regulatory Commission's (NRC) review and approval. The addenda document changes FCF's currently approved methodology, BAW-10133P, Revision 1 (Reference 3), for analyzing fuel assembly loading during seismic and loss-of-coolant accident (LOCA) conditions in pressurized water reactors (PWRs). Both addenda address modifications to the horizontal LOCA and seismic models. No modifications to the original core bounce or fuel assembly vertical models were proposed. By letters dated January 4 and June 28, 2000, the NRC requested additional information regarding the addenda to the topical report (References 4 and 5). FCF provided additional information by letters dated March 17 and July 20, 2000, in response to the staff's requests for additional information (References 6 and 7).

2.0 EVALUATION

Addendum 1 proposed two modifications to currently approved methods (Reference 3) for modeling LOCA and seismic response of PWR fuel. The first proposed modification is a new method for modeling the stiffness of assembly grid locations. Section 2.1 of this safety evaluation provides the staff's evaluation of this proposed modification. Addendum 1 also proposed an alternate method of treating the fluid effects on fuel response. Previously, only added fluid mass was placed at grid nodes. The new proposed method also adds the effects of hydrodynamic coupling between core baffle plates and assemblies. Section 2.2 provides the staff's evaluation of this modification. Addendum 2 proposed the use of higher damping parameters for the modes involving seismic and LOCA responses. This is due primarily to the demonstrated damping influences of fluid flow in typical PWR operations. Section 2.3 provides the staff's evaluation of this modification. Pacific Northwest National Laboratory (PNNL) was a consultant to the NRC in this review.

2.1 Spacer Grid Dynamic Model

Addendum 1 describes a change in the structural model of the fuel assemblies to modify the nature of their response due to assembly-to-assembly impact at grid locations. This applies to the horizontal core model only, and no changes are being made for the vertical and core bounce model described in Reference 3. This modification essentially deals with the parameters K and C in Addendum 1. This modification will produce a more realistic response, especially when an assembly is struck (at a grid location) from opposite sides by adjacent assemblies or core baffle plates. The previously-used grid stiffness that is being revised is described in Appendix A of Reference 3, and the change involves only one K parameter and one C parameter for the horizontal model. The previous spring constant K was tri-linear, while the new method uses constant spring-constant values. The proposed model used experimental techniques that were similar to those used in the original approved methodology to obtain these parameters.

For the various K and C values in the proposed model, there were two constraint equations (Equations 3-11 and 3-12 of Addendum 1) based on a lumped parameter grid dynamic model (shown in Figure 3-1 of Addendum 1). One equation relates to the three stiffness parameters and another equation relates to the damping parameters. Test data from two separate dynamic tests, the dynamic crush test and the lateral pluck test, in conjunction with these constraint equations were used to supply information needed to acquire all K and C values.

The lateral pluck test was performed at room temperature. Data was later corrected for typical PWR accident conditions. The test used a prototype assembly with clamped end conditions typical of reactor core tie down conditions. The assembly was displaced at the center, released and allowed to impact rigid plates at various grid locations. Dynamic load and displacement time history data were taken for a variety of initial mid-span displacements. A computer model was constructed and used to model the various tests with various values of K and C. The values that best matched the experimental data were chosen. Since the mass associated with each grid element was known, this also yielded the damping ratio. These room temperature values were scaled to values reflecting accident conditions by assuming that the stiffness was proportional to Young's modulus values and also by assuming that the damping ratio was temperature invariant. The staff considers this approach acceptable based on the conservative assumptions.

It should be noted that the system damping due to reactor water does not play a role in these values. Damping due to reactor water is treated differently by selecting specific modal damping parameters for consideration. Thus, the fact that the pluck testing was done in air rather than water does not invalidate the data because the K and C values do not consider fluid effects. The staff considers this approach conservative and thus acceptable. Modal damping due to fluid effects is discussed in Section 2.3 of this safety evaluation.

Based on the conservative assumptions and acceptable test results, the staff concludes that the spacer grid dynamic model described in Addendum 1 to Topical Report BAW-10133P, Revision 1 is an adequate model for modeling fuel assembly and baffle plate impacts at grid elevations for seismic and LOCA analysis.

2.2 Hydrodynamic Coupling Model

The proposed model is described in Sections 2.2.2.1 and 2.2.2.2 of Addendum 1. A more detailed description is contained in Attachment 2 of Reference 6. The later reference provides much greater technical detail of the coupling model. The original approved core model of Reference 3 did not assume any hydrodynamic coupling between the baffle plates and the fuel assemblies. The fluid effects were simply treated by adding mass to the beam nodes to match experimentally determined natural frequencies. Core baffle plate motion would only load the outer assemblies and then only if the corresponding gaps between fuel assemblies and core baffle plate were in the closed position.

The proposed model is much more realistic than the one described in Reference 3. In addition to adding mass to the assembly beam nodes (different masses from those of the original model), coupling between the core baffle plates and each of the assemblies is treated by applying a load vector based upon the core baffle motion time history and information from a separate fluid flow model.

This fluid flow model represented a two dimensional (horizontal) slice of an assembly array. For the model concerned, flow was assumed to be non-viscous and incompressible, which is a conservative approach. For small motion amplitudes, the governing equations for this fluid motion results in a Laplace's equation which can be readily solved to yield velocity and pressure distribution in the fluid. Results from this model are then used to arrive at mass terms to be added to the assemblies and to the baffle in cases where loads on the baffle consist of force versus time histories. The analysis showed that there was very little assembly-to-assembly hydrodynamic coupling. The staff considers that assumption of non-viscous and incompressible fluid flow is conservative and thus acceptable.

FCF performed audit calculations of dynamic loading cases simulating safe shutdown earthquake (SSE), surge line break (SLB), and safety injection line break (SILB). Both horizontal loading directions were considered. In Reference 6, impact forces using the proposed model were compared to those generated by using the currently approved model of Reference 3. The results showed that there is a reduction in maximum grid forces for the relatively long duration of SSE. However, there were no significant differences for the SLB and SILB cases as compared to the previously approved model. Thus, the hydrodynamic coupling is considered to have minimal effect on the combined loading of seismic and LOCA on fuel assemblies. Based on the small change in combined loading when compared to the approved model, the staff considers the audit calculations to be acceptable.

Furthermore, the seismic responses using the proposed model were compared with those from the approved model and with test results. The proposed model provides conservative results relative to the test results, and is in better agreement with the test results than the approved model. Thus, the proposed model provides a more realistic approach to evaluating the accident conditions.

Based on the realistic approach, conservative assumptions, and acceptable audit calculations, the staff concludes that the hydrodynamic coupling model proposed in Addendum 1 to Topical Report BAW-10133P, Revision 1 is acceptable for seismic and LOCA analysis.

2.3 Fuel Assembly Damping Values

The fuel assembly dynamic response model described in the approved methodology (Reference 3) is based on an assumption of Rayleigh equivalent damping technique. This assumption is widely used in practice and is implemented by assuming that the damping matrix is a linear combination of the mass and stiffness. The two involved weight functions were determined from two natural frequencies and corresponding damping ratios. Addendum 2 proposed to modify the Reference 3 model by increasing the damping ratios to account for axial flow conditions. Although this could produce lower impact loading on fuel assemblies, it has been observed that such axial flow patterns indeed exist in simulated flow tests.

FCF has performed a substantial amount of fuel assembly damping testing, as was reported in Addendum 2 and in Attachment 1 of Reference 7. In addition to testing for the effects of flow rate on damping, FCF also studied other effects including temperature, dynamic amplitude, and hydrodynamic coupling in air testing environment. Testing facilities included the Control Rod Drive Line facility, a test facility called FAME at FCF's site, and the Hermes test loop facility in France. The FAME facility performs in-air resonance testing only. The FAME and Hermes facilities are capable of full-scale flow testing. All facilities employ appropriate mounting techniques to simulate in-reactor structural conditions.

There were three modes in the damping ratio in the approved methodology. However, only the first and third mode damping ratios contributed to the loading, while the second mode damping ratio had no effect on the loading. The first mode damping ratio was calculated from pluck testing and measurements of the decay of successive oscillations, which is also called the log decrement method. At all the test facilities, the results showed that the first mode damping ratio had test values higher than the value used in the approved methodology for typical PWR accident conditions. The proposed value for the first mode is slightly higher than the value in the approved methodology and still below the test values. The staff considers this increase acceptable because a conservative margin is maintained.

For the third mode damping ratio, in-air resonance testing was performed. The test results indicated that the damping ratios of the first and third modes were very similar. The proposed value for the third mode is also slightly higher than the value in the approved methodology, but still below the test values. The staff considers this increase acceptable because conservative margin is still maintained.

The combined effect of the slightly higher first and third mode damping ratios results in reduced seismic loads as expected, but little change in LOCA loads. Thus, the net effect of the combined seismic and LOCA loads will not significantly vary from the previous results in the approved methodology. Based on the applicable test facilities results, the conservative margins maintained, and the small effect on the overall analysis, the staff concludes that the proposed values for the first and third mode damping ratios are acceptable for seismic and LOCA analysis.

3.0 CONCLUSION

The staff has reviewed Addendum 1 and Addendum 2 to Topical Report BAW-10133P, "Mark-C Fuel Assembly LOCA-Seismic Analyses," Revision 1 and concludes that both addenda are acceptable for incorporation into the overall methodology described in BAW-10133P, Revision 1, for seismic and LOCA licensing applications.

4.0 REFERENCES

1. Framatome Cogema Fuels, "Submittal of Topical Report BAW-10133P, Rev. 1, Addendum 1, Mark-C Fuel Assembly LOCA-Seismic Analyses," September 30, 1997.

2. Framatome Cogema Fuels, "Addendum 2 to BAW-10133P, Rev. 1 Mark-C Fuel Assembly LOCA-Seismic Analyses," May 5, 1999.

3. Shah, S. J., Lide, R. E., "Mark-C Fuel Assembly LOCA–Seismic Analyses," BAW-10133PA, Rev. 1, June 1986.

4. Letter from Stewart Bailey to T. A. Coleman, "Request For Additional Information – Framatome Topical Report BAW-10133P, Addendum 1, Mark C Fuel Assembly LOCA-Seismic Analysis, Revision 1 (TAC No. M99906)," January 4, 2000.

5. Letter from Stewart Bailey to T. A. Coleman, "Request For Additional Information – Framatome Topical Report BAW-10133P, Addendum 2, Mark-C Fuel Assembly LOCA-Seismic Analysis (TAC Nos. M99906 and MA5902)," June 28, 2000.

6. Framatome Cogema Fuels, "Responses to Nuclear Regulatory Commission Questions on BAW-10133P, Revision 1, Addendum 1," March 17, 2000.

7. Framatome Cogema Fuels, "Responses to Nuclear Regulatory Commission Questions on BAW-10133P, Revision 1, Addendum 2, Mark-C Fuel Assembly LOCA and Seismic Analysis," July 20, 2000.

Principal Contributor: S. Wu

Date: October 17, 2000

ABSTRACT

The following addendum provides Framatome Cogema Fuels (FCF) with an alternate mechanical faulted condition method, which will eventually be phased in for all fuel assembly designs. Only the horizontal core model is modified from the previous core model described in FCF topical report BAW-10133P, Rev 1. FCF has modified core modeling techniques and spacer grid testing methods to be consistent with that of FCF parent company Framatome (FRA). The most significant changes are in the representation of the spacer grid and the coupling between assemblies and core baffle plates into the core model. The modeling of the spacer grid has been changed from a single impact spring (single load path) for each grid to in-grid (composite fuel rod to grid stiffness) and through- grid (grid external stiffness) representations for each grid (dual load path). The modeling of the hydrodynamic coupling has been changed from an added water mass at the assembly to incorporation of coupling that exists between assembly and core baffle plates.

The aim of this addendum is to outline the method for building the lateral core models used for the fuel assembly mechanical seismic and LOCA analysis. In order that the results of the analytical methods may be evaluated on a numerical basis, typical results of seismic and LOCA analyses are also presented.

TABLE OF CONTENTS

Page

1.0 INTRODUCTION 1-1

2.0 SEISMIC and LOCA LATERAL ACCIDENT MODELS DESCRIPTION

2.1 Introduction 2-1
2.2 Fuel Assembly Lateral Model 2-1
2.2.1 Assembly Model in Air, Cold 2-2
2.2.2 Assembly Model in the Reactor Environment 2-3
2.2.3 Row Model 2-7

3.0 IMPACT MODEL CHARACTERIZATION

3.1 Principle 3-1
3.2 Assembly Row Model 3-2
3.2.1 Principal of Row Impact Model 3-2
3.2.2 Determination of Grid External Stiffness and Related Damping 3-3
3.2.3 Row Configuration-External Springs 3-4
3.2.4 Internal Springs 3-5
3.2.5 Case of Hetrogeneous Rows 3-5
3.2.6 Intermediate Mass- Beam Model Correction. 3-5
3.3 Dynamic Crush Test 3-6
3.4 Lateral Pluck Test with Impacts 3-6

4.0 FA SEISMIC-LOCA ANALYSES RESULTS

4.1 Structural Configuration 4-1
4.2 Input Motions 4-1
4.3 Analysis Input 4-1
4.4 Analysis Results 4-5

5.0 CONCLUSION. 5-1

6.0 REFERENCES 6-1

Page

APPENDIX

A. CASAC CODE DESCRIPTION A-2

B. FUEL ASSEMBLY SEISMIC TESTS B-2

C. RESPONSE TO NRC QUESTIONS C-1

List of Tables

Table

3-1 Spacer Grid Dynamic Crush Test Results 3-8
4-1 Core Model Structural Parameters 4-7
4-2 Spacer Grid Impact Force Under Seismic and LOCA Loading 4-8

List of Figures

Figure

2-1 Single Fuel Assembly Beam Model for an 8-Grid Assembly 2-9
2-2 Horizontal Core Seismic and LOCA Model 2-10
2-3 Arrangement of Hyrodynamic Coupling Elements 2-11
2-4 Core Lateral Model 2-12
3-1 Impact Model at a Grid Location for a Single Assembly 3-9
3-2 Equivalent Grid Impact Model 3-9
3-3 Row Model for a Single Elevation 3-10
3-4 Dynamic Model for Simulating Fuel Assembly Lateral Impact Test 3-11
4-1 Upper Core Plate SSE-X Direction Horizontal Displacement Time History 4-9
4-2 Lower Core Plate SSE-X Direction Horizontal Displacement Time History 4-10
4-3 Baffle Plate at Upper Core Plate Elevtion 4-11
4-4 Upper Core Plate Safety Injection Line-X Direction Horizontal Displacement Time History 4-12
4-5 Lower Core Plate Safety Injection Line-X Direction Horizontal Displacement Time History 4-13
4-6 Baffle Plate at Upper Core Plate Elevation Safety Injection Line Break-X Direction Horizontal Displacement Time History 4-14
4-7 Assembly Structural Model Geometry 4-15

1.0 INTRODUCTION

The methods and models used in the FCF 17x17 fuel assembly design and other FCF fuel assembly designs for LOCA and seismic dynamic analyses were described in the topical report, "Mark-C Fuel Assembly Seismic and LOCA Analyses, Revision 1," BAW-10133P (Reference 1). The fuel assembly structural evaluations and methodology specific to the FCF Mark-BW 17x17 fuel assembly are provided in the topical report, "Mark-BW Mechanical Design Report," BAW-10172P (Reference 2). The safety criteria and methodology used for acceptable cycle reload analyses specific to the FCF Mark-B 15X15 fuel assembly are provided in the topical report, "Safety Criteria and Methodology for Acceptance Cycle Reload Analyses," BAW-10179P (Reference 11). All these reports have received the NRC approval for referencing in licensing applications. The following addendum provides an alternate method of seismic and LOCA analysis to be consistent with those used by the FCF parent company Framatome (FRA). This method allows for more accurate representation of fuel assembly dynamic response mainly by considering the effects of fuel rod to grid interaction and the hydrodynamic effects of reactor coolant. Although, the application of this method is for generic use (all FCF fuel assembly designs), its first use will be for licensing the next generation of FCF 17X17 fuel for Westinghouse designed reactors. The value of FCF adopting FRA's methodology is that a common test facility and test results can be used for licensing. Only the horizontal core model is modified-the fuel assembly vertical models remain the same as described in BAW-10133P, Rev.1.

The FRA grid impact test methods and LOCA/Seismic models are different from the FCF methods described in BAW-10133P, Rev.1. The following summarizes the differences.

1. FRA impacts a mass against the spacer grid, which is stationary against an anvil. The elastic "external" stiffness, peak impact load, and buckling deformation are determined. The test is generally stopped soon after the velocity required to buckle the grid has been reached.

2. FCF impacts the spacer grid (and rod segments) mass against an anvil. In effect, the elastic and plastic "internal" stiffness are determined along with the peak impact load (elastic) and additional impact load strength in the plastic range.

3. Otherwise, the types of data taken during the test are similar between FRA and FCF including, impact velocity, rebound velocity, impact loads, impact duration, damping, etc. (damping is calculated from test data).

4. FCF current treatment of the grid stiffness is appropriate but conservative. FCF currently does not use the fuel rod-to-grid stiffness (in-grid) in the seismic and LOCA analysis. This stiffness is determined by fuel assembly impact tests against a wall. The in-grid stiffness models the fuel rod local bending stiffness and the flexibility of the hard/soft stops support in the cells to the fuel rod. The modeling of the spacer grid will be changed to represent

both in-grid and through-grid impact loading as represented by the FRA methodology.

5. The primary coolant in the current (FCF) method is simulated by masses added to the assemblies. These masses are determined from the frequencies obtained by dynamic tests in air and in water. This method does not permit representation of the coupling between assemblies and with the baffle walls. This addendum incorporates a fluid interaction model which allows for actual coupling between assemblies and with the core baffle plates. The fluid interaction model development is based on seismic tests conducted on a shaker table by the Commissariat a' l' Energie Atomique (CEA.), in conjunction with Framatome, on groups of interacting assemblies.

The objective of this addendum is to outline the method for building the lateral models and to provide a general presentation of the analyses to evaluate the loads applied on the fuel assembly structure in accident conditions. The characteristics of the models are derived from the various mechanical tests on the fuel assembly, spacer grid, and shaker table tests. These are discussed in this report.

In order that results of the analyses may be evaluated on a numerical basis, typical results of seismic and LOCA analyses are presented. Horizontal seismic [b,c,d] and LOCA displacement time histories of the upper and lower core plates and of the core baffle plate at the upper core plate elevation for all the design cases developed for the Trojan plant were used as input conditions in the seismic and LOCA conditions analysis provided.

2.0 SEISMIC AND LOCA LATERAL ACCIDENT MODELS DESCRIPTION

2.1 INTRODUCTION

This report provides the mechanical faulted analysis methods planned to be used in licensing analyses by FCF, as an alternate to the current faulted conditions analysis methods. The application will be for all FCF fuel assembly LOCA and seismic dynamic analyses.

A flow chart of the analysis remains the same as given in the previous report (Reference 1). The horizontal core model has been modified, to allow the simulation of in-grid and through-grid impact loading. The method for building this model is outlined, and in order that the results of the analysis methods may be evaluated on a numerical basis, specific results are presented.

2.2 Fuel Assembly Lateral Model

A lateral accident model represents a row of fuel assemblies, excited by input displacements and velocities at its boundaries. The lateral modelization of the fuel assembly to simulate its dynamic behavior is shown in Figure 2-1. This individual model is duplicated to represent any number of fuel assemblies in a given row in the core.

This model consists of beam and rotational springs having the free vibrational characteristics of the fuel assembly. A set of one dimensional dynamic elements is incorporated at each spacer grid location (spring, dash-pot and gap), which act when the assembly impacts occur at the grid level.

The characteristics of these various elements are benchmarked to the results of extensive testing, which include the following measurements:

- fuel assembly lateral stiffness
- vibrational features of the fuel assembly (natural frequencies, mode shapes, damping)
- grid behavior under lateral loading
- assembly behavior under lateral impact.
- fuel assembly dynamic behaviour under F/A mock-ups tests subjected to seismic excitation on a shaker table.

The results of the lateral stiffness test and of the free vibrational characteristics of the fuel assembly enable the rotational springs characteristics to be determined.

Two types of elements are used to simulate the various impact conditions on the fuel assembly. When the grid impact compression is applied between the two opposite sides of the grid, the elements noted (K_E and C_E: external grid characteristics) shown in Figure 2-2 are acting. Their characteristics are obtained from the impact tests on grids. When only one grid side is loaded by the impact, the other type of elements (Ki and Ci; internal grid characteristics) are also acting.

Their characteristics are finally determined by comparison with the results of the fuel assembly lateral impact tests.

In the fuel assembly row models for the existing methodology [1], the primary coolant was simulated by masses added to the assemblies. These masses were determined from the frequencies obtained from dynamic tests on assemblies in water. As part of this topical report, FCF has modified the core modelling method, which now incorporates hydrodynamic coupling between assemblies and baffles. The graphic representation of the coupling elements is shown in Figure 2-3.

This coupling model is based on analytical estimation, which is globally validated by interacting fuel assembly mock-up tests performed in water.

The model determined above is assembled to form a row of a given number of fuel assemblies in the core (usually fifteen). An assembled model of a row of assemblies is shown in Figure 2-4. In the seismic or the LOCA analysis this core row model is loaded by input displacements and velocities at its boundary; i.e., lower and upper core plates at the bottom and top nozzles and core baffle plate at the grid levels. These input data come from the reactor system analysis. The time duration of the analyses is generally [b,c,d] for the LOCA and between [b,c,d] for the seismic. The dynamic analysis is performed using the computer program CASAC Appendix A).

The model building approach follows three main phases, described below.

2.2.1 Assembly Model, in Air, Cold

This part of the assembly modeling remains basically unchanged from the present methodology [1]. However, a brief description of the model is provided below to provide certain basic features of the model construction method.

The mass nodes are located at the intermediate spacer grid locations. The model representing the assembly lateral deformations consist of the numerical sum of the cross sectional inertias (bending stiffness and shear stiffness) for the fuel rods, guide thimbles and instrument thimble, and rotational springs. Initial rotational spring stiffnesses are calculated from mechanical properties of the fuel assembly spacer grids obtained from the spacer grid springs (hard-stops and soft-stop) load-deflection test data. The model is one-dimensional with two degrees of freedom per node (translation and rotation). The fuel assembly contains eight grids; however the end grids are considered as integral parts of the end supports (nozzles); hence, these are not modeled. Figure 2-2 represents an 8-grid assembly design model.

Two tests are primarily used in the dynamic model development. The first, a fuel assembly pluck test, is performed on a prototype fuel assembly in air and in water at room temperature to obtain

fundamental frequency and damping at various amplitudes. The pluck test is conducted by measuring and recording the displacements of selected spacer grids as the fuel assembly is deflected laterally at the midplane and quickly released. The second test, a shaker test, is performed on a prototype fuel assembly in air to obtain the first six frequencies and mode shapes of the fuel assembly. The initial rotational spring stiffnesses are then adjusted until the dynamic model duplicates the shaker test frequencies, as accurately as possible. Although the shaker test only provides data for the fuel assembly in air, this data provides a basis to establish the correct rotational spring stiffnesses.

While pluck test data are used in the fuel assembly model development, a lateral static analysis is also performed with the fuel assembly model in 70°F air to assure that the lateral stiffness matches that obtained from the lateral static deflection tests.

2.2.2 Assembly Model in the Reactor Environment

The method for review does not use an in-water model as with the existing faulted method. The in-water model is obtained from in-water frequency measurements on a single assembly. Even though, this model is conservative, it is unable to take into account coolant effects on a sufficiently realistic basis. The bases for the new model benchmark are shaker table tests. Even in the absence of axial flow, the shaker table tests are more significant as described in Appendix B. They provide overall validation of a model based on in-air dynamic characterization and on fluid coupling analytical estimation.

2.2.2.1 Hydrodynamic Model Phenomenon and Consistency

The presence of a dense fluid in contact with structures modifies their vibrational response. The nonstationary interaction between an ideal fluid and a structure constitutes the hydrodynamic coupling, a non-dissipative phenomenon, which is distinct from damping. In the linear form applicable to small motions, the relationship between pressure forces and structural accelerations is classically represented by an added mass matrix, proportional to fluid density.

For a set of submerged structures and the fluid containment excited simultaneously, the model must be capable of describing the near-static response, practically modeled as a rigid motion for the coupling. In these conditions, the resulting load applied to a structure can be written :

$$f = -(m-m_d)\gamma(t) \qquad (2\text{-}1)$$

where m is the mass of the structure, m_d is the displaced fluid mass, and $\gamma(t)$ is the entrainment acceleration. The effect is analogous to buoyancy force; it produces a decrease in the applied inertia force, and not an increase by "added mass". This principle implies a relationship between added mass matrix terms and allowance for all the non-negligible couplings, particularly the one

with the containment. This coupling is similar to that between solids described by Fritz (Reference 5) and between rectangular plates more explicitly described by Scavuzzo et al. (Reference 9).

2.2.2.2 Model Hypotheses and Properties for PWR Assemblies

The coupling is defined in a horizontal plane between cross-sections of assembles or core baffles assumed non-deformable, This assumption is consistent with the beam structural model. The values of the terms are linear, per unit length height, which are discretized in proportion to the modeled height, like the structural mass.

The basic hypothesis of the coupling model can be formulated in two ways as follows:

1) the analyzed assembly row is laterally confined, therefore hydraulically independent of its neighbors, and:
2) the motions of the rows parallel to motion direction are identical.

The calculations are performed with fluid finite element models, by resolving the Laplace equation by thermal analogy. The results show that the coupling possesses the following properties:

- it is negligible between assemblies.
- it is uniform, namely:

  - the mass term added to each assembly, [c], and the coupling term between the assembly and baffles, [c], are practically independent of the assembly position in the row,

  - the contribution of each fuel rod to the coupling terms is practically independent of its position (which makes extrapolations to a complete assembly far easier, see section 2.2.2.3).

The model can then be defined for any assembly "in a reactor environment", with two terms linked by the consistency relationship:

$$[b,c,d \qquad\qquad] \tag{2-2}$$

where [c] is, as defined in Eq. (2.1), the displaced fluid mass. The absence of couplings between structures except with the containment also implies that the effect of reducing the applied inertia forces given by Eq. (2-1) remains valid for any dynamic response.

Although hardly intuitive, the coupling properties can be clearly interpreted by the confinement effect. The lateral confinement hypothesis tends to be justified by both analytical considerations

and the full-scale validation of the models by in-air and in-water shaker table tests described in Appendix B. Further discussion on the interpretation of the fluid interaction model coupling terms is provided by Rigaudeau et al. (Reference 10).

2.2.2.3 Actual Determination and Allowance for the Coupling

The fluid finite element calculations are performed to define the coupling terms in a dimensionless form, relative to the displaced fluid mass.

The inputs to the CASAC fluid-structure elements are determined as follows:

1) Definition of the non-dimensional values of the assembly added mass, [c,d], and of the coupling with the baffles, [c,d]. These values verify a relation analogous to Eq. (2.-2):

[b,c,d] (2-3)

2) Calculation of corresponding linear values:

[*b,c,d*] [*b,c,d*]

where [*b,c,d*] is the linear water mass displaced, assumed to consist only of fuel rods, i.e :

[*b,c,d*]

where [c]: fuel rod outer diameter
[c]:average coolant density in a fuel assembly for a given reactor condition
[c]: number of fuel rods per row (array nxn)

3) Calculation of values attributed to model nodes. For a node of index i:

[*b,c,d*] [*b,c,d*]

where [*b,c,d*] is the assembly height assigned to the node, which in practice is the average of the lengths of the adjacent beam elements.

4) Input into the coupling elements, whose primary node corresponds to an assembly node [c,d] and the secondary node [c,d], to a baffle node located at the same height:

[*b,c,d*] = primary mass
[*b,c,d*] = coupling mass

The secondary mass is not factored in as the baffle motion is imposed.
For a 17x17 array assembly, the dimensionless values derived from a fluid model are

[b,c,d] [b,c,d] (2-4)

and the displaced mass represents about [b,c,d] of the structural mass.

For other fuel assembly arrays, the reduced pitches are similar to those for 17 x 17, and the above values constitute good approximations. For categorical justification of the mechanical strength in accident conditions, it is nevertheless preferable to recalculate the values with a fluid model for a given fuel assembly array.

2.2.2.4 Influence of Axial Flow and Deflection

Fuel assembly frequency and damping are determined at [b,c,d] inch lateral deflection because it is a conservative approximation (damping increases with increasing deflection and frequency is an inverse function of deflection) of the gap between fuel assemblies in core. From the testing, it is shown that fuel assembly damping increases significantly with increasing flow rate.

Fuel assembly structural damping values corresponding to a minimum operational design flow rate were conservatively chosen for Safe Shutdown Earthquake (SSE) and Loss of Coolant Accident (LOCA) conditions. The % critical damping values are [c,d] for the first mode and [c,d] for the higher modes. The results of the tests and their interpretation in fact point to these damping values being rather conservative, in particular that of the first mode.

2.2.2.5 Input into the Assembly Model: Rayleigh Damping

The fuel assembly structural damping is modeled as a combination of the mass and stiffness matrices, i.e., it uses Rayleigh damping in the form:

$$C = \alpha\,[M] + \beta\,[K] \qquad (2\text{-}5)$$

where α and β are determined from two given damping ratios that correspond to two unequal frequencies of vibration. The reduced damping of mode i is given by:

$$\xi_i = \frac{\alpha}{4\pi f_i} + \beta\pi f_i \qquad (2\text{-}6)$$

where: ζ_i = damping ratio
f_i = frequency

The coefficients α and β are derived from Equation (2-6), applied to two modes i and j of given frequency and damping.

$$\alpha = \frac{4\pi f_i f_j(\xi_j f_i - \xi_i f_j)}{f_i^2 - f_j^2} \tag{2-7}$$

$$\beta = \frac{(\xi_i f_i - \xi_j f_j)}{\pi(f_i^2 - f_j^2)} \tag{2-8}$$

The frequency values must of course be considered for the reactor environment, and therefore are determined by modal analysis with hydrodynamic coupling.

The coefficients α and β are determined from mode 1 and that of a close higher mode (generally mode 3) determined from the tests for a [b,c,d] inch deflection of the assembly.

Determination of the first mode parameters (frequency and damping) is the easiest with respect to amplitude, as the pluck test can be directly used. The situation is more problematic for mode 3 as the amplitude is often limited with the shaker test, and is not directly comparable with that of mode 1. For frequency and damping, the simplest method is the rule of extrapolation as follows:

$$[b,c,d \qquad\qquad] \tag{2-9}$$

where [b,c,d] corresponds to the small amplitudes [b,c,d].

2.2.3 Row Model

To create the core model, the single fuel assembly model development described in sections 2.2.1 and 2.2.2 is taken and a model of a row of assemblies in co-planner fashion is developed using the computer program CASAC (Reference 3).

The core model requires the addition of 'external" and " internal" grid stiffnesses at each intermediate spacer grid location.

The intermediate mass "m", shown in Figure 2-4, has a value close to that of the grid, but is slightly higher for numerical reasons. For the impact core model, this mass is removed from the

fuel assembly mass and introduced as a stand alone mass.

The gaps between grids of adjacent fuel assemblies and the baffles are determined, which completes the core model.

Usually, the longest row of fuel assemblies in the core envelopes all row configurations Nevertheless, the principle of the model building approach is applicable to any row length of the core.

FIGURE 2-1

Single Fuel Assembly Beam Model for an 8-grid Assembly

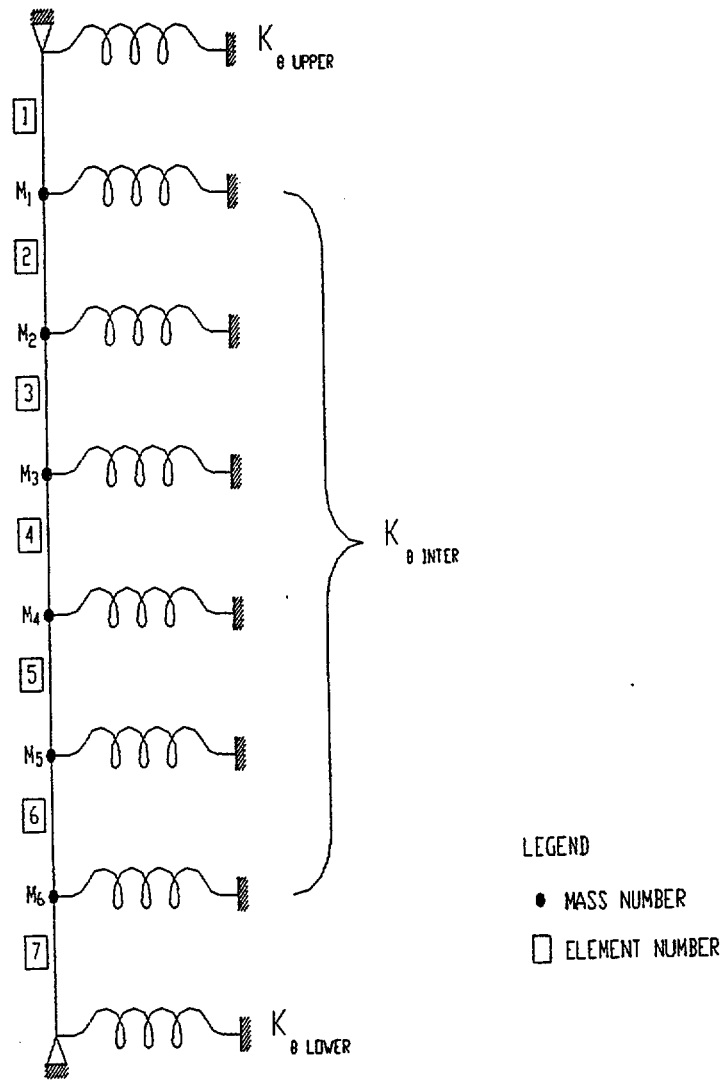

FIGURE 2-2

Horizontal Core Seismic and LOCA Model

[b,c,d]

FIGURE 2-3

Arrangement of Hydrodynamic Coupling Elements

[b,c,d]

FIGURE 2-4

Core Lateral Model

[b,c,d]

3.0 Impact Model Characterization

3.1 Principle

The fuel assembly impact behavior is investigated from lateral pluck tests with impact on grids. The fuel assembly model developed for "free" motion is used to simulate the lateral pluck impact test.

The "equivalent local dynamic stiffness", K_{eq}, and "equivalent local dynamic viscous damping", C_{eq}, are determined by choosing the values to provide agreement between the measured grid impact forces in the test and those from the model simulation. In fact, the values for stiffness, K_{eq}, and viscous damping factor, C_{eq}, are not independent. The value, C_{eq}, is defined by:

[*b,c,d*] (3-1)

In other words, it corresponds to the same reduced damping [c] as the external stiffness [c] of the grid (see section 3.2.2) on the basis of the span mass [c,d].

This procedure means considering K_{eq} as a grid-linked stiffness, whereas it corresponds much more to overall dynamic behavior (not reflected by the beam model) than to a local bearing stiffness.

The equivalent local dynamic stiffness K_{eq}, and equivalent local dynamic viscous damping C_{eq}, obtained from the fuel assembly lateral impact tests performed in air at room temperature (70°F), are corrected for the average reactor operating temperature (600°F). For the impact model, equivalent local dynamic stiffness K_{eq} is corrected by the ratio of Young's modulus (hot and cold). The Zircaloy mechanical material properties are used.

[*b,c,d*] (3-2)

Given the definition in Eq. (3-1) of the equivalent local dynamic viscous damping factor C_{eq}, it is corrected to the square root of K_{eq}:

[*b,c,d*] (3-3)

These corrections are the only ones performed to allow for the reactor environment. The impact model is unaffected by the coolant effects.

3.2 Assembly Row Model

3.2.1 Principal of Row Impact Model

In a row of the core, several assemblies are likely to find themselves simultaneously in contact. For an assembly, contact may occur at the same time on two opposite sides of one or several grids. The model is designed to cover two types of force transfer.

1) From or to the assembly, with an equivalent impact model (K_{eq}, C_{eq}) determined as described in section 3.1.

2) Through the assembly, i.e., one or several of its grids, using a grid [b,c,d] stiffness K_E and associated damping C_E. Unlike the equivalent impact parameters, K_E and C_E are grid-specific, for compression between its two opposite faces, and are obtained from dynamic compression crush tests. The parameters K_E and C_E are defined as the stiffness and damping at the point when the crush limit is obtained.

The combination of these two models yields the complete impact grid model shown in Figure 3-1 for a single assembly. In this model:

- the two stiffnesses $2K_E$ and damping values $2C_E$ in series correspond to K_E and C_E, between opposite faces of a grid

- the "internal" stiffness [b,c,d] in series correspond to K_{eq}, while [b,c,d] in series correspond to C_{eq}, between a beam node and a grid face (as shown in Figure 3-2).

- the intermediate mass m is needed for explicit numerical integration. The intermediate mass m, which represents the grid mass, is small compared with the mass of a span. However, it enables the principles of series positioning of adjacent stiffnesses to be applied, even in dynamic mode, and has a negligible effect on the assembly beam model.

Note that in practice:

[b,c,d]

[b,c,d]

In other words, the [b,c,d] model parameters in fact play the role of equivalent impact parameters.

3.2.2 Determination of Grid External Stiffness and Related Damping

The dynamic crush tests are conducted at 600°F, by impact at increasing velocities of a mass equal to the mass of a span. Before buckling, the results obtained in the elastic range enable the stiffness and damping to be determined on the basis of a single spring mass-damper model.

Use is made of the "energy" method, where the stiffness K_E is given by:

[*b,c,d*] (3-4)

[*b,c,d*] (3-5)

where:
[c,d] = maximum force during impact,
[c,d] = impacting mass corresponding to span mass,
[c,d] = impact velocity,
[c,d] = velocity coefficient of restitution.

Determination of the grid external properties is performed through the following procedure:

1) The term [c,d] is obtained from the slope of the straight part of graph [c,d] = [c,d], divided by [c,d].

2) The term [c] is derived from the damping coefficient term [c], which is obtained from the impact force work.

This gives:

[*b,c,d*] (3-6)

[*b,c,d*] (3-7)

The relationship given by Equation (3-6) is approximate but quite acceptable for small damping [b,c,d].

The term [d] is determined as an average for the same impacts used in [c,d] determination.

Given the mutual dependence between stiffness and reduced damping in the above relationships, an iterative process using Equations (3-4) through (3-7) is used:

[b,c,d]

] (3-8)

The convergence is very fast since it is obtained better than [b,c,d] iterations.

3.2.3 Row Configuration - External Springs

The grid impact model of external springs is represented in Figure 3-1 for one grid of a single assembly and in Figure 3-3 for the set of grids with the same vertical level in the assembly row in its final form. It is seen from Figure 3-1 that in the assembly row the springs [b,c,d] of neighboring assemblies are in series. They can therefore be replaced by a single spring [b,c,d], with the springs [b,c,d] only remaining between outer assemblies and baffle plates. The configuration of the structural row model is given in Figure 2-4, where the springs are represented by the conventional scheme of their stiffness only.

For the two stiffness values, two corresponding average gap values may be used: the inner-assembly gaps, which are considered identical, and outer assembly and baffle plate gaps.

These gaps are determined by the following relationships:

Between Assemblies: [b,c,d] (3-9)

Between Outer Assemblies and Baffle Plates:

[b,c,d] (3-10)

where [b,c,d] grid width (distance between opposite faces)
[b,c,d]: pitch between assemblies
[b,c,d]: distance between opposite baffle plates, at the end of the row
[b,c,d]: number of assemblies in the row

These values are for hot conditions.

Finally, the characteristics of two types of nonlinear springs and corresponding gaps are input:

[b,c,d] (between assemblies)

[b,c,c] (between outer assembly and baffle plate, at the ends)

3.2.4 Internal Springs

According to the model principles in section 3.2.1:

[b,c,d] (3-11)

[b,c,d] (3-12)

where the values of [c,d] and [c,d] are defined at hot condition as described in section 3.1.

3.2.5 Case of Heterogeneous Rows

Each type of assembly has equivalent grid impact characteristics [b,c,d], external grid characteristics [b,c,d] and subsequently internal grid characteristics [b,c,d] defined from the relationships given by Equations (3-11) and (3-12).

When a gapped spring is located between two identical assemblies, or between outer fuel assembly and baffle plates, it is defined as above; which defines [b,c,d], and the gap value through the grid width [c,d](relationships given by Equations 3-9 and 3-10).

If the gapped spring is located between two different assemblies, types "1" and "2", the following relationship results:

[b,c,d] (3-13)

[b,c,d] (3-14)

[b,c,d] (3-15)

3.2.6 Intermediate Mass- Beam Model Correction

The intermediate mass is called "grid mass" but its value is slightly higher for numerical reasons. The typical value is slightly more than [b,c,d]. This value is quite small with respect to span mass.

The existence of this mass requires the reduction of the total mass of the assembly beam model by

an equivalent amount to keep the assembly structural mass the same.

3.3 Dynamic Crush Test

Dynamic crush tests are performed to determine the grid "external" characteristics of the Zircaloy intermediate spacer grids as discussed in section 3.2.2. The grid external stiffness (through-grid stiffness K_E), damping, and allowable impact loads are determined from these tests and used as input to the horizontal core seismic and LOCA model. Spacer grids are tested at [b,c,d]. The results of the spacer grid dynamic crush tests used are provided as a reference example in Table 3-1.

The test spacer grid is horizontal and secured on one face (outer strap) to a very rigid frame, with the other faces free to move. The spacer grid is supported with four longer rods on the peripheral row leaning against the anvil. Each grid is filled with empty fuel rod and guide thimble segments. A mass impacts the grid at the opposite face. This mass is generally equivalent to that of an assembly span [b,c,d]. The test involves gradually increasing the impact velocity until grid instability takes place, which allows characterization of the grid behavior within the elastic range. The crush limit loads are found at the point of instability. Impact force, impact duration, pre-impact and post-impact velocity are measured during each impact. This data is input into a single degree of freedom model using the energy method to calculate equivalent dynamic stiffness and damping values. (The stiffness and damping are determined from the impact energy data).

The failure mode of the spacer grids is typically racking in the outer three rows and the guide thimble positions are not altered. During the test, a control rod insertability test is performed in order to follow the guide thimble array deformation trend.

After grid instability occurs (i.e., when the maximum load decreases for 2 successive impact), the grid is subjected to subsequent constant higher impacts to examine the grid post-buckling behavior in the plastic energy range. During the test, the control rod insertion inspections are made after each impact in order to follow the guide thimble deformation trend.

3.4 Lateral Pluck Test with Impacts

The purpose of this test is to determine a value for the "equivalent impact dynamic stiffness and damping " of the spacer grid as these values are used as input to the fuel assembly horizontal core model as explained in sections 3.1, 3.2.1 and 3.2.4. The test is performed in air at ambient temperature. In the test, the prototype fuel assembly is constrained at both ends representative of the reactor-core tie-down condition. For the reference example test, the prototype fuel assembly featured [b,c,d]. The test consisted of imposing a certain known deflection at a center grid location, then released against one or more impact plates so that the prototype impacted against a rigid wall. Initial gaps between grids and corresponding impacting plates were simulated to represent the inner-assembly or outer fuel assembly and baffle gap before imposing the lateral

displacement. The lateral displacement and impact forces at mid span grid levels were continuously recorded versus time during the test.

Three different conditions of impact were considered (Grid positions are shown in Figure 3-4): [b,c,d].

In addition to varying the selection of impact grids as described above, the total fuel assembly displacement at the center grid location was varied. Displacements of [b,c,d] were tested and the corresponding impact forces were measured.

In order to determine the internal spacer grid stiffness, single fuel assembly finite element models (cold in-air) of the test cases described above were conducted. The model consisted of a series of beam elements, rotational springs, and translational springs. For each model, the center grid was plucked the specified displacement, then allowed to impact a stationary object. A sketch of the model used to benchmark against the impact forces found in the testing is shown in Figure 3-4. The resulting impact force was compared to the test data. The translational spring stiffness was then varied until a match was obtained between the calculated impact forces and those determined during testing. The process was repeated for all cases and the spacer grid equivalent local dynamic stiffness and damping were determined.

The process yielded the following parameters :

K_{eq}= [b,c,d],
ζ_{eq} = [b,c,d].

Table 3-1

Spacer Grid Dynamic Crush Test Results

Test Temperature	Average Stiffness (Lbs./in)	Average Damping Ratio	Average Maximum Elastic Force (lbs.)
[		b,c,d	]

FIGURE 3-1

Impact Model at Grid Location For a Single Assembly

[b,c,d]

Figure 3-2

Equivalent Grid Impact Model

[b,c,d]

FIGURE 3-3

Row Model For a Single Elevation

[b,c,d]

Figure 3-4

Dynamic Model for Simulating Fuel Assembly Lateral Impact Test

[b,c,d]

4.0 FA Seismic-LOCA Analyses Results

This section provides an example of the application of the methods described in sections 2.0 and 3.0 of this addendum report. Included are detailed model inputs, input seismic and LOCA displacement time histories, and representative analysis results of the Mark-BW 17x17 fuel assembly.

4.1 Structural Configuration

The model (Figure 2-4) consisting of a row of beams connected by spacer grid impact models (Figure 3-1), is built readily from CASAC structural elements: beams, external nonlinear and internal linear translational springs, and lumped intermediate masses. This model is located in an XY plane, where X is the horizontal direction and Y is the vertical one. The model comprises of degree of freedom's (d.o.f's) only for displacement UX and for rotation RZ for the beam (the axis perpendicular to the model plane).

4.2 Input Motions

Usually, from the reactor system analysis, the displacements and velocities of the upper and lower core plates and baffle plates are known. If only the displacements are supplied, the velocities can of course be derived from the displacement data using the numerical differentiation.

4.3 Analysis Input

This section provides description of the example reference faulted condition analysis, including the specific values used in the computer analysis input, and the specific seismic and LOCA forcing functions used in the analysis. For the horizontal direction, the seismic and LOCA analyses are performed for two orthogonal horizontal directions, namely for the X and Z directions.

4.3.1 Faulted Condition Time Histories

The seismic time histories of the upper and lower core plates and of the core baffle plate developed for the Trojan plant for the [c,d] Safe Shutdown Earthquake (SSE) were used in the fuel assembly seismic analysis. These displacement time histories for the upper core plate, lower core plate and baffle plate at the upper core plate elevation joints for the horizontal X direction are shown in Figures 4-1 through 4-3, respectively. The horizontal SSE-X direction provided the highest seismic loading condition.

The LOCA input time histories used were taken from the Trojan Plant reactor system analysis. The Portland General Electric Trojan Plant was licensed for Leak-Before-Break (LBB). This analysis considers the worst case Trojan Plant LBB LOCA breaks; namely, a [c,d] surge line guillotine and a [c,d] safety injection line guillotine. Figures 4-4 through 4-6 respectively provide

the calculated upper core plate, lower plate and upper baffle plate horizontal [c]-direction displacements for the safety injection line break. The safety injection line break for the [c] direction provided the highest horizontal LOCA loading condition.

The fuel assembly model parameters that are presented are of a Mark-BW fuel assembly; however, the method of analysis used is applicable in general to all FCF fuel assembly fuel designs.

4.3.2 Beam Model- Geometry and Mass

The model scheme and position of the nodes are defined in Figure 4-7. Note that a Mark-BW 17x17 fuel assembly has a total of 8 grids only, of which 6 are represented by intermediary nodes. The two end grids are integrated into the top and bottom nozzles in the model.

The beam cross section is the total cross section of the 264 fuel rods, 24 guide thimbles and one instrument thimble. The moment of inertia of the fuel assembly is calculated by taking the bending stiffness of the fuel assembly and dividing by the modulus of elasticity for the fuel rod material. Since the moment of inertia for the guide thimbles is not the same for the lower and upper parts due to different cross sectional areas, a different value for the fuel assembly moment of inertia for lower and upper parts of the assemblies is calculated. The moment of inertia for the fuel assembly above the guide thimble dashpot region is [b,c,d]. The moment of inertia for the fuel assembly below the guide thimble dashpot region is [b,c,d]. Since the upper inertia is the larger area over the much larger length of the fuel assembly, it is used as input into the CASAC model. The cross-sectional properties used as input at [b,c,d] are:

Moment of Inertia= I = [b,c,d]

Area =A = [b,c,d]

Shear coefficient = k = [b,c,d]

4.3.3 Spacer Grid Assembly Weight

The spacer grid weight is utilized in the core model by CASAC to determine the mass distribution of the fuel assembly weight at each of the model nodes. The weights of the Mark-BW intermediate grids are:

Vaned: [b,c,d].
Vaneless: [b,c,d].

In the Mark-BW design, the five upper intermediate spacer grid assemblies employ flow mixing vanes on the downstream edges (top), adding slightly to the total weight.

To ensure the model numerical stability, CASAC requires a slightly higher lumped mass value at each grid position than just the grid weight. Thus, the distribution used is

Grid	Mass (lbs)
1	[c,d]
2	[c,d]
3	[c,d]
4	[c,d]
5	[c,d]
6	[c,d]

Total Grid Weight = [b,c,d .]

The Mark-BW fuel assembly weight in water at 600^0 F (which includes the hydrodynamic water weight) used for analysis is [b,c,d]. The total fuel assembly weight used in the calculation of the assembly density is then:

[b,c,d]

4.3.4 Rotational Stiffnesses

To match the frequency and lateral stiffness of the bench test , the rotational stiffness of the intermediate spacer grids is established. The rotational stiffness value obtained is:

Intermediate Spacer Grid Rotational Stiffness = $K_{\theta inter}$ = [b,c,d]

4.3.5 Density

The equivalent density of the fuel assembly is calculated by dividing the fuel assembly weight by the fuel assembly volume. The total weight used to determine the fuel assembly density is the wet weight above minus the sum of the modeled spacer grid assembly weight. The nozzle to nozzle guide thimble length is [b,c,d].

The equvalent density is:

$\rho = m/v = m/(AL)$

ρ = [b,c,d]

4.3.6 Element Lengths

The element lengths are used to define the vertical elevation of each span defined by spacer grid assemblies. The element length values listed below are from the centerline of the spacer grid assemblies. The term L_1 is the length from the top nozzle to the first intermediate grid below it. The term L_7 is the length from the bottom nozzle to the first intermediate grid above it. The seven element lengths are:

L_1 = [b,c,d]
L_2 = [b,c,d]
L_3 = [b,c,d]
L_4 = [b,c,d]
L_5 = [b,c,d]
L_6 = [b,c,d]
L_7 = [b,c,d]

4.3.7 Clearance Dimensions

Fuel Assembly to Assembly Gap, at [b,c,d] = [b,c,d]
Outer Fuel Assmembly to Baffle Plate Gap, at [b,c,d] = [b,c,d]

4.3.8 Material Properties

The mechanical properties of the Zircaloy at [b,c,d] are:

Modulus of Elasticity = E = [b,c,d]

Poisson's Ratio = υ = [b,c,d]

4.3.9 Fuel Assembly Structural Damping

As defined in section 2.2.2.5, the value for the Rayleigh coefficients of damping are:

α = [b,c,d]s^{-1}
β = [b,c,d]s

4.3.10 Impact Equivalent Model

The grid equivalent stiffness is determined by assembly impact tests against a wall as described in

section 3.4. The grid equivalent stiffness and viscous damping values determined by benchmarking the impact loads produced by CASAC with the impact values determined through fuel assembly lateral impact testing are:

k_{eq} = [b,c,d] lbs/in.

ζ_{eq} = [b,c,d]

4.3.11 Grid External Stiffness and Related Damping

The dynamic compression tests discussed in section 3.3 provided the following average values.

K_E = [b,c,d] lbs/in.

ξ_E = [b,c,d]

4.3.12 Hydrodynamic Coupling

4.3.12.1 Definition of non-dimensional values

The non-dimensional values (i.e. related to the displaced water mass) of the mass added to the assembly, [*b,c,d*] and of the term of coupling to the core barrier, [*c,d*], are defined for the 17X17 fuel assembly in section 2.2.2.3 of this report as:

[*b,c,d*] = [b,c,d] [*b,c,d*] = [b,c,d]

Linear values of the coupling elements are calculated first as outlined in section 2.2.2. The average density of the primary core coolant under operating conditions is used. The coupling values attributed to the nodes are therefore calculated by multiplying the linear values by the associated height, half-sum of the lengths of the adjacent elements.

All values used as structural input to the core model are summarized in Table 4-1.

4.4 Analysis Results

Spacer Grid Impact Forces Under Seismic and LOCA Loading

The fuel assembly seismic and LOCA analyses were performed using the CASAC code for both the horizontal X and Z directions. The core model developed in sections 2 and 3 was run with the seismic and LOCA time histories described above. The object of the analyses was to determine the maximum elastic force in the grid locations. The resulting maximum impact forces subjected to the Trojan time histories are listed in Table 4-2. The maximum grid impact forces obtained

from the SSE analysis and LOCA analysis were found to be within the spacer grid elastic load limit as determined by the spacer grid dynamic crush tests given in Table 3-1. The loads for LOCA plus SSE were combined by the square-root-of-sum-of-squares (SRSS) methods discussed and accepted by the NRC in Reference 4, "NUREG-0800, Standard Review Plan 4.2, Appendix A." No permanent deformation of the grid was shown for any of the seismic and LOCA cases; hence the loads are acceptable.

Table 4-1 Core Model Structural Parameters

[b,c,d]

Table 4-2 Spacer Grid Impact Force Under Seismic and LOCA Loading

[b,c,d]

FIGURE 4-1

Upper Core Plate SSE-X Direction Horizontal Displacement Time History

[b,c,d]

FIGURE 4-2

Lower Core Plate SSE-X Direction Horizontal Displacement Time History

[b,c,d]

FIGURE 4-3

Baffle Plate at Upper Core Plate Elevation SSE-X Direction
Horizontal Displacement Time History

[b,c,d]

FIGURE 4-4

Upper Core Plate Safety Injection Line -X Direction
Horizontal Displacement Time History

[b,c,d]

FIGURE 4-5

Lower Core Plate Safety Injection Line Break -X Direction
Horizontal Displacement Time History

[b,c,d]

FIGURE 4-6

Baffle Plate at Upper Core Plate Elevation Safety Injection Line Break
- X- Direction Horizontal Displacement Time History

[b,c,d]

Figure 4-7

Assembly Structural Model Geometry

[b,c,d]

5.0 Conclusion

FCF has modified modeling techniques for the detailed horizontal core model and spacer grid impact testing methods so as to 1) produce more realistic faulted loadings and 2) to converge the mechanical faulted methods used in licensing analysis by FRA (FCF parent company) and FCF. Specifically the modeling of the spacer grid has been changed to represent both "in-grid" and "through-grid" stiffnesses. The FCF modified lateral core modeling technique is similar to the industry standard methodology. Detailed descriptions of each phase of building the lateral accident core model are provided. The model qualification method outlined in this report provides an assurance of the behavior of the core model under seismic and LOCA loading conditions.

A hydrodynamic coupling model based on the fuel assemblies row lateral confinement has been incorporated and is justified from calculations and seismic tests. Thus, the undue conservatism of the models comprising of a single added mass at each assembly is eliminated. A complete qualification procedure during the core model building leads to a model behavior which is conservative in the overall validation under seismic and LOCA loads. The core model building methodology is thoroughly qualified, and the model is shown to provide more representative loading of the fuel assembly.

A detailed horizontal core response analysis was performed under combined seismic and LOCA loads. The seismic time histories of the upper and lower core plates as well as of the core baffle plate developed by FCF for the Trojan plant for the [b,c,d] Safe Shutdown Earthquake was used in the fuel assembly seismic analysis. The input time histories for the LOCA were taken from the Trojan Plant reactor system analysis. This analysis considered the worst case Trojan Plant leak-Before-Break(LBB) LOCA breaks; namely, a [c,d]surge line guillotine and a [c,d]safety injection line guillotine. The horizontal loads for the LOCA plus SSE were combined by the square-root-of-the-sum-of-squares (SRSS) as discussed and accepted by the NRC in the Standard Review Plan 4.2, Appendix A, NUREG-0800. The loads calculated for SSE plus LOCA were compared to the elastic load limit of the Mark-BW spacer grid. The spacer grid impact loads for all faulted conditions were within the spacer grid elastic load limit. Therefore, no permanent grid deformation was predicted and the coolable geometry requirements were shown to be met.

The current methods provided in Reference 1 are sufficient for meeting the safety margins. However, the development of methods presented in this report provides more realistic fuel assembly behavior and can be utilized as an alternate method for licensing the fuel assembly.

6.0 References:

1. BAW-10133P, Rev 1, Mark-C Fuel Assembly LOCA-Seismic Analyses, Topical Report, June, 1986.

2. BAW-10172P, Mark-BW Mechanical Design Report, July, 1988.

3. FTG-TM-113. Orig. CASAC Structural Design Program, November 1996.

4. NUREG 0800, USNRC, "Standard Review Plan, " Rev. 2, July 1981.

5. Fritz, R.J., "The Effects of Liquids on the Dynamic Motions of Immersed Solids" ASME Journal of Engineering for Industry - February 1972 - Page 167-173.

6. Ralson, A. Mathematical Methods for Digital Computers, Wiley, Newyork/London, 1969, Page- 95-109.

7. Ralson, A. " Runge-Kutta Methods with Minimum Error Bounds " MTCA, vol. 16, n "80-1962-Page 431-437.

8. ANSYS Engineering Analysis System, Swanson Analysis Systems, Inc., Version 5.2, Users manual.

9. Scavuzzo R.J., Stokey W.F., Radke E.F., , Dynamic Fluid Structure Coupling of Rectangular Modules in Rectangular Pools, 1979, PVP 39, 77-86.

10. Rigaudeau J., Brochard D., Benjedidia A., 1993, Fluid Structure Interaction in the Response of PWR Fuel Assemblies to Horizontal Seismic Loads, SMIRT 12, Stuttgart, K 17/5.

11. BAW-10179P-A, Rev. 1, Safety Criteria and Methodology for Acceptance Cycle Reload Analyses, Framatome Cogema Fuels, February 1996.

APPENDIX A

CASAC Code Description

APPENDIX A

A.1 CASAC Code Description

The CASAC code was developed by Framatome (FRA) in order to evaluate the dynamic behavior of fuel assemblies subjected to loading resulting from a Loss of Coolant Accident or from an earthquake. The response of the fuel assembly to such loadings takes the form of highly non-linear behavior, whether laterally due to the presence of inter-grid gaps or vertically due to the rod-grid connection mode.

CASAC is a finite element code for calculating the response of structural models made up of different elements. The elements incorporated in CASAC are beams, rotational springs, translational springs, sliding elements, contact elements, fluid-structure coupling elements and lumped masses. The fluid-structure coupling element simulates the effects of hydrodynamic coupling between two structures. The coupling element operates as a corrector of the mass matrix ("added mass matrix") as described by R.J. Fritz (Ref. 5).

The loading can be applied at several degrees of freedom in the form of sinusoidal excitation, accelerations or forces versus time and in the form of boundary conditions expressed as velocities and displacements. The CASAC analysis types include:

- static analysis
- modal analysis
- response spectrum analysis
- dynamic analysis
- non-linear static

In the non-linear dynamic analysis, the CASAC computer program analyzes two types of structural model:

- Firstly, models featuring beams interconnected by stiffnesses (translation or rotation springs), sliding elements, contact elements, or fluid/structure coupling elements. These elements simulate the lateral behavior of structures or of mechanical equipment.

- Secondly, "mass-spring" models which generally allow analysis of the axial behavior of mechanical systems.

Dynamic analysis determines the behavior of a structure subjected to loads with respect to time. Dynamic equilibrium at each step is given by:

- nodal displacements, velocities and accelerations,
- the state of non-linear elements,

- loads and stresses in the elements.

CASAC uses an explicit integration scheme.

The CASAC non-linear transient dynamic analysis solution capability is used in the fuel assembly seismic and LOCA analyses. The dynamic equilibrium of a system is expressed by the equation:

$$[M](\ddot{X}) + [C](\dot{X}) + [K](x) = (F(t)) \qquad \text{(A-1)}$$

where [M] is the mass matrix,
[C} is the damping matrix,
[K] is the stiffness matrix,
(X) is the displacement vector,
(X) is the velocity vector, and
(F(t)) is the external force vector.

As matrix [M] is positive definite, Equation (A-1) can be written as

$$(\ddot{X}) = [M]^{-1} (F(t) - [C](\dot{X}) - [K](X)) \qquad \text{(A-2)}$$

Taking (V) as the velocity vector, relationship (A-2) is equivalent to:

$$\frac{d(X)}{dt} = (V)$$

$$\frac{d(V)}{dt} = [M]^{-1} (F(t) - [C](V) - [K](X))$$

By introducing the velocities as independent unknowns, now a system of N second order differential equations, has been transformed into a system of 2N first order differential equations.

From the numerical point of view, the integration of the differential equations system is achieved by the HAMMING predictor-corrector method (Ref. 6), with initialization using the RUNGE-KUTTA method (Ref. 7).

A brief description has been presented showing the general principle used in CASAC. Details of the general methods used in CASAC to solve transient dynamic problems are given in Reference 3.

Program Qualification

A verification calculational report has been prepared for the CASAC program which compares CASAC calculated solutions with exact analytical solutions or with another finite element

program (ANSYS- Ref. 8). The guidelines of Quality Assurance (QA) procedure BWNT-0903-03 governing development and control of software documentation were followed in the preparation of the validation report. Three problems were checked in detail to ensure that the CASAC results were correct and the CASAC results matched with the ANSYS results or the theoretical answers. In all cases, very good agreements [b,c,d] were found for the results of test cases run.

In addition, the qualification of CASAC is ensured by FRA through a set of test-cases providing optimum coverage of software capabilities. Test cases included real models relating to the fuel assembly design, which included both modal and dynamic analysis.

APPENDIX B

Fuel Assembly Seismic Tests

APPENDIX B

Fuel Assembly Seismic Tests

B.1 Introduction

The models of a fuel assembly row, which are used in the study of the PWR core seismic behavior, are now qualified by means of out of core tests performed with single assemblies. But the model validity can be completely verified only with seismic tests on groups of interacting fuel assemblies.

Such seismic tests have been conducted on a shaker table by the Commissariat a' l' Energie Atomique (C.E.A.), in conjunction with Framatome, on sets of interacting fuel assembly mock-ups. The tests were performed in air and in water, with a confinement simulating the core baffles, and using accelerograms generated from a seismic design basis spectrum. The tests were performed on 5-mock-up row, 13-mock-up row and 13 mock-up in diamond shaped pattern.

The overall program included the following phases:

- dynamic and impact characterization of several full-size assemblies;
- development and characterization of a reduced-scale mock-up;
- analysis of the response of a core featuring five or thirteen reduced-scale mock-ups in a row pattern (see Figure B-1) to uniaxial seismic loading, and thirteen reduced-scale mock-ups in diamond-shaped pattern (see Figure B-2) to biaxial seismic loading, in air and in water.

This appendix reports the main experimental results obtained for the second phase (tests on three configurations of mock-ups).

B.2 Description of the Mock-Ups

Since the facilities did not allow simultaneous testing of several full-scale mock-ups (on board mass too high), Framatome has designed reduced scale mock-ups with the mock-up resonance frequencies close to typical of full-scale assemblies, but with a mass [b,c,d] smaller.

Some components and dimensions of these mock-ups were identical to those of the full-scale items, such as rods (diameter, cross-section and materials), guide thimbles, certain grid characteristics (thickness, cross-section , rod span) and grid span. To reduce the mass while maintaining the frequencies, the rod array was reduced to a [b,c,d] pattern, with [b,c,d] and [b,c,d], and the number of grids was [b,c,d].

Before these seismic tests were performed, dynamic characterization tests were performed on full-scale mock-ups and on these reduced scale mock-ups. These tests enabled validation of these

mock-ups, for which first frequencies, damping and their variations versus excitation level were measured.

B.3 TEST PROGRAM

Tests were performed with several configurations (see Table B.1), each with a different environment, gap between fuel assembly mock-ups, and number of mock-ups.

Table B.1

Environment*	5 Mock-ups Row	13 Mock-ups Row	13 Mock-ups in Diamond-Shaped Pattern*
in air	gap: [c,d] gap: [c,d]	gap: [c,d]	gap: [c,d]
in water without confinement	gap: [c,d] gap: [c,d]		
in water with confinement	gap: [c,d] gap: [c,d]	gap:[c,d]	gap: [c,d]

* Note: (5 rows of 1, 3 and 5-mock-ups with confinement similar to that of core baffle plates - Figure B-2)

For each row configuration, the excitation consisted of:

- sine sweeps at low level (maximum acceleration 0.025g to 0.2 g)
- increasing seismic excitations (0.1g to 0.6g) with one or several accelerograms (test at 0.4g was repeated 5 times).

For the diamond pattern mono-axial and bi-axial (two orthogonal horizontal X and Y directions) seismic excitation corresponding to a specified spectrum was used. The specified spectrum was chosen such that a peak of the acceleration centered on the primary natural frequency of the real assemblies.

The objective of the this test program was to obtain information on:

- influence of the fuel assembly total number on impact forces

- influence of the gap between fuel assemblies
- influence of the environment: water effects and confinement effects
- influence of the accelerogram signals
- scattering of the results

For the diamond pattern, the objective of the test program was to also study the influence of bi-axial excitation on fuel assembly impact forces and displacements.

B.4 Description of the Test Facility

The seismic tests were performed at C.E.A. on the mono-axial shaker table for the row configuration and on the bi-axial table for the diamond pattern The mono-axial shaker table [b,c,d] was driven by an electrohydraulic actuator of [b,c,d]. The maximum permissible mass on the table was [b,c,d]. The bi-axial shaker table [b,c,d] was driven by an electrohydraulic actuator of [b,c,d] with the maximum permissible mass [b,c,d].

The test rig was bolted on the shaker table as shown in Figure B-3.

The dimensions of the rig were:

- height = [b,c,d]

- length = [b,c,d]

- mass = [b,c,d]

The row (5 or 13 mock-ups) was placed in the rig and the gap [b,c,d] between each mockup was adjusted. A load cell was mounted on the baffle plate at each end of the row, at each grid elevation [b,c,d].

Slotted baffle plates allowed a lateral water confinement for the mock-up row (see Figure B-3).

The test rig was comprised of lateral removable panels, made of plexiglass for viewing the mock-up motions and checking the instrument behavior during tests.

The mock-ups were restrained at top and bottom with 4 alignment pins, and no vertical force was applied to the top during seismic tests.

B.5 Instrumentation

The instrumentation allowed (see Figures B.2 and B.4) measurement of:

- acceleration of the table
- acceleration on top of the rig
- displacement of all the mock-ups
- impact forces on the grids for the 2 mock-ups located at the row ends

Special displacement sensors were developed to resolve space and water-tightness problems.

B.6 Main Tests Results

For each test, the studied parameters were:

- the maximum impact force obtained at each of the twelve instrumented grid locations;
- the sum of these maximum impact forces, for the 12 grids all together, or for 6 on each side;
- the force integral with time;
- the average impact duration.

These parameters were studied as a function of the environment conditions, and level of excitation.

B.7 Main Results

All parameters examined increased with the excitation level. Maximum forces were reached at mid-height (grid no. 3 and 4).

The tests conducted with 5-mock-ups in the row, in air and in water, with and without confinement showed that:
- with confinement, the effect of water is much higher, since a [c,d] decrease at [c,d] of the impact force integral values was observed.

The tests at [c,d] and [c,d] between each assembly showed that the impact force integral is higher for the [c,d] configuration than for the [c,d] configuration. This was because the smaller the gap, the greater the number of impact points, and less the assembly distortion. However, the peak forces were higher for [c,d] than for [c,d], since for large gaps, the displacements and accelerations which occurred were higher.

The model qualification was performed on the 5 mock-up row, the 13 mock-up row and the 13 mock-up in the diamond shaped pattern. Figures B.5 presents the in-water maximum impact forces which compares with the analytical model predictions (with fluid coupling and added mass) for the test results of the 5 mock-up row , either single (monoaxial) or in the bi-axial (diamond-shaped) pattern. Figure B.6 presents the in-air and in-water maximum impact forces which compares with the analytical model (with fluid coupling and added mass) predictions for the 13 mock-up row test results. The model is found conservative, yet more realistic for the consistent

coupling model than with the single added mass model. The coupling model is justified from its global coherence with the observed effects.

FIGURE B-1

Fuel Assemblies Confinement

[b,c,d]

FIGURE B-2

Layout of Diagonal-Shaped Pattern

[b,c,d]

FIGURE B-3

Test Rig

[b,c,d]

FIGURE B-4

Fuel Assemblies Instrumentation

[b,c,d]

FIGURE B-5

Maximum Impact Forces For In-Water 5 Mock-Up Rows

[b,c,d]

FIGURE B-6

Maximum Impact Forces In The 13 Mock-Up Row

[b,c,d]

APPENDIX C

Response to NRC Questions

RESPONSES TO NUCLEAR REGULATORY COMMISSION QUESTIONS ON BAW-10133P, REVISION 1, ADDENDUM 1

1. Page 2-6, Section 2.2.2.4, states that damping increases significantly with increased axial flow. No data could be located in Addendum 1 for axial flow conditions used for damping investigations. Please provide any additional data that relates to the effect of axial flow on damping.

   Response

   The fuel assembly damping values were established from in water tests at conditions that simulated the complete range of reactor operating flow conditions. The effect of flow rate on the fuel assembly average percent critical damping derived from full-scale fuel assembly tests is shown in Figures Q1.1 and Q1.2. Figure Q1.1 was given in the original topical report BAW 10133PA, Rev. 1 (Figures 4.1 and 4.2 of Question 4).

   Addendum 2 of BAW-10133P, Rev.1 was submitted to the NRC on May 17, 1999, which justifies the use of higher damping values in the fuel assembly seismic and LOCA models. All the relevant data for the use of higher damping values including Figures Q.1.1 and Q.1.2 are provided in the Addendum 2 report.

2. The bottom of page 2-7 states that the intermediate mass "m" is slightly greater than that of a grid "for numerical reasons." Please elaborate. Was this done for numerical stability?

   Response

   The use of a slightly greater mass than that of the actual grid results in the reduction of the mass of the assembly beam model. The overall mass of the assembly remains the same. The benefit of using a slightly higher mass is the improvement in the model run computation time. FCF has performed CASAC runs with actual grid mass [b,c,d], and no numerical instability problem was experienced. In fact, it was found in the analysis results that this change in the grid mass has no effect on the grid forces or on the model behavior.

   CASAC uses an explicit numerical integration method. Effective stability is ensured by an automatic error control, which is usually kept significantly smaller than those required for impact description.

3. Appendix B gives some interesting results comparing the "hydrodynamic model" with the "masses added" model that was used previosly. Were both of these models using the "newer" grid stiffness model? Please provide comparisons with the current model and the model that was previously used (i.e., without the

Addendum 1 modifications). Has it been shown that the new model bounds the data (i.e., over-predicts damage) including uncertainies in the data?

Response

All the test results presented in Appendix B were obtained by FRAMATOME. A comparison with test results using the "newer" grid model clearly shows that although the "hydrodynamic model" is effectively less conservative than the "mass added" model, the model results still remain notably conservative with respect to tests. It is shown in Appendix B of Addendum 1 (Figures B.5 and B.6) that the new model bounds the maximum in-water impact forces obtained from the fuel assembly seismic test programs for all level of seismic excitations (0.1 g to 0.6g). The influence of the coupling model has not been studied with the "older" grid model, yet it is very likely that similar trends would be obtained, since fluid coupling is exerted on the assembly lateral deformations, with no direct connection with the impact model at grid levels.

4. On page 3-1 (equation 3-3), the temperature scaling of equivalent damping makes use of temperature dependent stiffness (Young's modulus) ratios. Please explain the physical reason for this approach. Please substantiate the temperature independence of percent critical damping, or provide justification why this approach is adequately conservative.

Response

Single grid impact tests were performed at room temperature and at 600^0F. The test results indicate that the temperature does not seem to affect the spacer grid structural damping, ζ_E.

In the pluck test with impact on grids which provides the equivalent impact parameters (K_{eq}, C_{eq}), the impact force signal is very similar to that of a single span mass M_{sp} impacting the equivalent stiffness K_{eq}. Then the spring-mass model of Section 3.2.2 is applicable. The calculation of the spring viscous damping is performed with the following relationship as given by Equation 3-1 in Addendum 1.

[b,c,d] (1)

For the impact model, equivalent stiffness K_{eq} is corrected by the ratio of Young's modulus (hot and cold). Given the definition of the spring viscous damping (Equation 1) and as the spacer grid structural damping is not temperatue dependent, the temperature scaling of the spring viscous damping leads to Equation 3-3 (viscous damping C_{eq}, proportional to the square root of K_{eq}) given on page 3-1 of Addendum 1.

More generally, the damping values associated with the impact stiffnesses do not have much influence as long as they remain within a reasonable range. In any

case, this influence is much smaller than that of the assembly damping introduced in the beam.

5. On page 3-3 (equation 3-6), the parameter Π is not defined. Please elaborate on the derivation of equation 3-6.

Response

The parameter not defined (Π) is the upper case of π (typographical error). This mathematical constant will be corrected in the final submission of Addendum 1. All the equations are derived from the response of the mass-spring-damper oscillator with initial zero deflection and initial velocity V_I. The impact ends when the net force in the spring-damper and therefore the mass acceleration vanish.

Equation 3-6 corresponds to the usual exponential damping factor:

[b,c,d]

where ω is the pulse of the undamped oscillator, and t is equal to the impact duration, such that :

[b,c,d]

which means that the impact duration is slightly shorter than a half-period. Equation 3-6 is approximate, but the approximation is quite satisfactory for small damping [b,c,d].

6. Page 2-6 states that alpha and beta are chosen in order to give the desired values of critical damping for the first mode and all higher modes. Please provide further justification for selecting the value of critical damping that was used for all higher modes.

Response

The damping values for the first and higher modes are provided in section 6 of Addendum 2 of BAW-10133P, Rev. 1. These values were obtained from the shaker modal tests, which were performed in air at room temperture. The damping values recorded were at very low amplitude. Based on the shaker table test results, the first mode and higher modes damping values are [b,c,d]. Therefore, using [b,c,d] damping value for the higher modes [b,c,d] is conservative.

The recent (November 1999) resonance tests performed at CEA in water under axial flow conditions on the Framatome fuel assembly clearly show that [b,c,d] damping (at least) for the higher modes is justified. This data is still in the process of documentation.

It may also be noted that in accident studies, there is less impact of the damping value for higher modes than for the first one. Effectively, the first mode is predominant in the seismic response. For the LOCA response, the contribution of higher modes is enhanced but the influence of damping is notably minimized in this very short transient, without sustained oscillations.

7. From the data on Table 4-1, it appears that fuel mass was considered in your model (by increasing the density of beam material), but fuel stiffness was neglected. This lack of fuel stiffness consideration appears to be the primary reason for requiring rotational stiffness elements at the beam nodes in order to match experimental results. Please explain why this approach is valid for all intended uses of this methodology.

Response

In lateral deformation, the fuel assembly behavior exhibits a high-shear effect, i.e. the modal frequencies are close to integer multiples of the first one. This results from an individual bending of all the tubes (fuel rods, guide-thimbles and instrument thimble), restrained in grids which remain almost horizontal, i.e. their rotations are much smaller than in a global beam bending, in which they would remain perpendicular to the neutral axis.

A completely phenomenological modelling of such a behavior is not accessible to a single beam model, which implies that the parameters must be adjusted to match the experimental frequencies. However, there exist relationships with the described behavior. In particular :

- the cross-sectional inertia is the sum of those of the guide-thimbles and fuel rod claddings, without any supplementary term allowing for the distance to the neutral axis,
- the initial values of the rotational stiffnesses are related to the rod restraining conditions, and the connection of the springs to a fixed node provides a restriction to the absolute rotation of the grids, i.e. with respect to the horizontal.

Increasing Young's modulus is not equivalent to the rotational springs, since it involves increasing in the same ratio frequencies corresponding to a predominant flexion, with little shear. An alternative solution which proves acceptable is to increase the cross-sectional inertia while using an artificially small shear area in Timoshenko's beam formulation, but the model presented in Addendum 1 is more physical.

The density of the fuel assembly provided in Table 4-1 is calculated by dividing the fuel assembly mass by the fuel assembly volume. The fuel assembly length is taken as the nozzle to nozzle guide tube length.

Benchmarking of the fuel assembly modeling in air remains unchanged from the previous modeling (section 2.2.1 of Addendum 1). In this part of the modeling,

the fuel assembly natural frequencies and lateral stiffness are benchmarked to the test results. To match the natural frequencies and lateral stiffness of the benchmark test, the rotational spring stiffness of the intermediate spacer grids are varied.

8. Please provide examples of licensing analyses of seismic and LOCA models for "limiting plant cases" comparing the new and old models.

Response

The maximum impact forces for "limiting seismic and LOCA time histories" generated by the new and old models are provided below. The input motion for the time histories as discussed in section 4 of BAW-10133P, Rev.1, Addendum 1 is given at the upper core plate, lower core plate, and upper baffle plate locations. The time duration of the analyses is [b,c,d] seconds for the seismic run and [b,c,d] second for the LOCA run. Three faulted conditions listed below were investigated.

It can be seen that the maximum impact forces generated by the new model are lower during the seismic event because of the incorporation of the hydrodynamic coupling and the new grid impact model into the core model. The impact forces generated by the new model during a LOCA, in two out of four faulted cases, are higher compared to the old model. From these results, it can be seen that incorporation of the hydrodynamic coupling has a strong effect on the fuel assembly seismic response (the total duration of the analysis is [b,c,d] seconds), and a small effect on the fuel assembly LOCA response (the total duration of the analysis is [b,c,d] seconds). The grid impact model used in the new model is consistent with that presently used by other fuel vendors.

b,c,d

Load Cases

SSE-X – Safe Shutdown Earthquake –X Direction
SSE-Z – Safe Shutdown Earthquake –Z Direction
SLB-X – Surge Line Break – X Direction
SLB-Z – Surge Line Break – Z Direction
SILB-X – Safety Injection Line Break – X Direction
SILB-Z – Safety Injection Line Break – Z Direction

9. The model described in B&W report BAW-10133PA was executed using the STARS code (1972, Ref. 1 of BAW-10133PA). The models described in the Addendum being reviewed are executed with the CASAC code (1996, Ref. 3 of BAW-10133P Addendum 1). Appendix A mentions that the CASAC code has been benchmarked against other finite element codes and closed form solutions. Are there issues with numerical instability, as discussed in Question 2 above, that result from use of the CASAC code? Please provide a copy of this verification report and provide justification that the switch in code usage does not require further review.

Response

Effective stability is ensured by CASAC as discussed in the response to Question 2.

[b,c,d]

The CASAC code has been extensively used by analysts at Framatome. All CASAC results are based on classical engineering concepts. In all test cases, very good agreements between the results of CASAC with exact form solutions or with the ANSYS results were found. (ANSYS is a widely used general purpose finite element program.)

The CASAC code has also been verified based on fuel assembly lateral pluck and impact test results.

The CASAC code has been certified by FCF in accordance with NRC-approved QA procedures.

10. References 5 and 9 of Addendum 1 were reviewed to gain background into the hydrodynamic coupling model. Flow models used in arriving at mass added parameters assume inviscid, irrotational, two-dimensional flow. It appears that the same flow model is used to arrive at "masses" regardless of node elevation. Please provide justification that this is suitable for nodes near the assembly ends.

Response

The reviewer's interpretation is correct that the same fluid model is used to arrive at "masses" regardless of node elevation, since this model is based on the two-dimensional flow hypothesis with a uniform flow pattern along the fuel assemblies. The two-dimensional flow hypothesis is based on the highly extended character of the structures, with lateral motions only (i.e. beam modeling), and negligible end effects.

The latter hypothesis is not specific to the proposed coupling model. It is implicit in the commonly used added mass model, in which the in-water frequency decrease observed in out-of-core tests is merely reflected by a uniformly increased beam mass.

For PWR fuel assemblies, negligible end effects are justified by the effectively very slender character of the structures, and more especially, since the most significant scaling length for the fluid flow is the rod pitch. (A good approximation of coupling is obtained with a model of a single rod cell as described in section 3.3 of Reference 10 of Addendum 1). In addition, coupling has no influence on the motions at assembly ends, which are input. For comparison, fuel storage racks in a pool are much less slender, and the rack tops are free to move next to a plenum, which leads to a significant vertical fluid motion and coupling decrease (see additional Reference 1A of this document-Enclosure 2).

11. Page 2-6 gives non-dimensional values for the assembly added mass and the coupling with baffles for a 17X17 assembly, and states the values are "derived from a fluid model." While these values are similar to those reported in Reference 10 of Addendum 1, no detail of the fluid model was given. Please provide details of the fluid model.

Response

The fluid model and its description are provided in Reference 1A of this document. Figure Q11.1 represents the schematic of this model, which comprises of a 3x3 array of 9x9 rod array assemblies. Figure Q11.2 represents the fluid mesh, reduced to the lower right quarter from symmetries with respect to the X and Y axes. As reported in Reference 10 of Addendum 1, the rod diameter – [b,c,d] and pitch [b,c,d] correspond to the 17x17 design. Gaps of [b,c,d] between assemblies or with the core baffles are included (average in-core value).

For the determination of the added mass term m_a, the lateral confinement of the rows along the motion direction X is obtained by accelerating simultaneously the center assemblies in the rows along X, i.e. the complete central row along Y. The

coupling term with the baffles m_c is not dependent on any hypothesis on the assembly motions, since it can be obtained from the baffle acceleration.

The dimensionless values of m_a and m_c are respectively equal to [b,c,d] and [b,c,d] for the assembly in center position. The sum is not exactly equal to [b,c,d], and the [b,c,d] difference reflects the small coupling with other assemblies. The calculated values are rounded-off and very slightly modified to fulfill exactly the consistency relationship, thus yielding the structural model values [b,c,d] and [b,c,d]. The very small decrease in absolute value with respect to those in Ref. 10 mainly results from the gap between assemblies.

Further details and analyses are given in Reference 1A.

12. It is the reviewers understanding (from reviewing Ref.10 of Addendum 1) that :

    a. The fluid coupling masses added to the assembly nodes were independent of assembly position in the model, and varied with grid number (Table 4-1) because of the differences in element lengths (as specified in 4.3.6). Please elaborate if this interpretation is not correct.

    b. Hydrodynamic coupling "between" assemblies was totally neglected. Please elaborate if this interpretation is not correct.

Response

The interpretations are absolutely correct.

Additional Reference :

1A RIGAUDEAU, J., Hydrodynamic Coupling in Seismic Response of PWR Fuel Assemblies and Other Immersed Structures, ASME-PVP Conference, Boston 1999, PVP-Vol. 394.

[b,c,d]

Figure Q1.1 FCF Mark-C 17 x 17 FA Average First Cycle Damping Under Flowing Conditions

[b,c,d]

Figure Q1.2 Damping Versus Effective Amplitude of Displacement

[b,c,d]

Figure Q11.1 Schematic of the Fluid Model Of a 3 X 3 Assembly Array

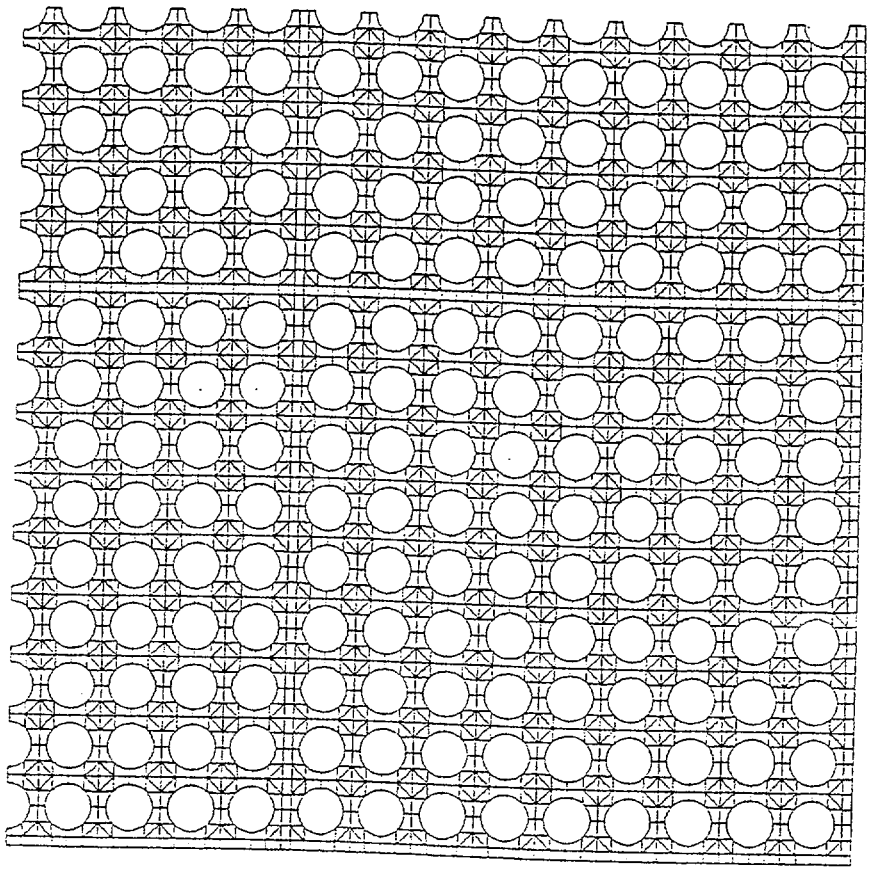

Figure Q11.2 Fluid Model of the 3 x 3 Assembly Array

Enclosure 1

[b,c,d]

CASAC Validation Report
[b,c,d]

Enclosure 2

PVP Conference Paper on Fuel Assembly Fluid Model

HYDRODYNAMIC COUPLING IN SEISMIC RESPONSE OF PWR FUEL ASSEMBLIES AND OTHER IMMERSED STRUCTURES

Jean Rigaudeau
FRAMATOME Nuclear Fuel
10, rue Juliette Récamier
69456 LYON Cedex 06, France
Phone : 33 4 72 74 88 37
Fax : 33 4 72 74 88 08
e-mail : jrigaudeau@framatome.fr

ABSTRACT

The influence of hydrodynamic coupling is not negligible in the seismic response of immersed structures, such as PWR fuel assemblies. The coupling basic features are first presented as guidelines to consistent modelling, in which the fluid containment plays an essential part. Finite element solutions are applied to plane coupling between highly extended structures. For the assembly single row model currently used in core seismic analysis, a coupling model based on the row lateral confinement proves very simple, and justified from calculations and tests. The case of fuel storage racks is considered for comparison and appears to be more complex for applications. Non linear effects are briefly discussed.

1. INTRODUCTION

In the response of PWR fuel assemblies to horizontal seismic loads, the influence of primary coolant is far from negligible. Unlike fluid-induced damping which is currently included in structural damping, allowance for the non-dissipative hydrodynamic coupling requires specific elements in the structural model. The aim of the paper is to show how a realistic and readily applicable model can be obtained from appropriate assumptions and calculations. The case of fuel storage racks is also considered but less extensively, in order to display the differences and similarities encountered in the coupling properties for various kinds of immersed structures. Except when otherwise stated, coupling is assumed linear, and the structures are considered as highly extended with perfectly rigid cross-sections (beam modelling), which leads to plane fluid models for coupling estimate. A typical description of such a coupling is given by Fritz (1972).

2. COUPLING FUNDAMENTAL FEATURES AND DETERMINATION

2.1. General equations and coupling effect

By assuming small motion amplitudes in an incompressible and non-viscous fluid, continuity and momentum transfer equations are linearized :

$$\mathrm{div}\,\vec{V} = 0 \tag{1}$$

$$\mathrm{grad}\,P = -\rho\frac{\partial\vec{V}}{\partial t} \tag{2}$$

where V, P and ρ stand for fluid velocity, pressure and density respectively. Therefore the pressure field is a solution of Laplace equation :

$$\Delta P = 0 \tag{3}$$

with boundary conditions corresponding to the structural acceleration component perpendicular to the solid surface (through eq. (2)). Coupling then results from the reciprocal action of pressure loads on structural motions, and for discrete models, the linear force-acceleration relationship leads to the well known added mass matrix concept :

$$F_{hydrodynamic} = -M_A\ddot{X} \tag{4}$$

where X is the structural displacement vector. For rigid structures and a single direction for motion and forces, each matrix term is defined by the resultant of pressure forces ($-m_{ij}$) on structure S_i generated by a unit acceleration of S_j, and vice-versa.

2.2. Physical interpretation

The fluid motion is entirely governed by continuity and may be considered from a purely kinematic standpoint. From linearity and commutativity of the space and time derivatives, the motion can be represented by the displacement, velocity or acceleration fields, all satisfying the continuity equation (1), with the corresponding potentials as solutions of Laplace equation (3). Advanced finite element formulations use the displacement potential for symmetry considerations

in generalized forms as described by Jeanpierre et al. (1979). Continuity macroscopic balances performed on velocity allow approximate solutions by applying Lagrange equations to the fluid kinetic energy, as presented by Scavuzzo et al. (1979) for rectangular shapes. Yet from a dynamic standpoint, acceleration is the only significant field since producing the resultant pressure forces through the pressure gradient (2). These forces are directly related to the magnitude of acceleration along the structures, unlike in the steady flow where the pressure gradient is related to that of velocity, and leads to zero forces on submerged bodies in an ideal fluid (d'Alembert's paradox).

Conversely, the non-stationary character is obvious from the added mass matrix representation, but the fluid kinematics should not be neglected. The concept of inertia is valid indeed for a fluid particle, or for global effects from the supplementary fluid kinetic energy : positive definite matrix and frequency decrease, sum of the matrix terms for one direction equal to the fluid mass (when completely bounded by the structures). But as the coupling terms individually represent hydrodynamic forces, they may be negative (when non-diagonal) and depend on the direction; above all, under confined conditions, they may become large with respect to the fluid mass, merely because in out-of-phase motions, the fluid acceleration is large when compared with the structural ones.

2.3. Consistency relationships for sets of immersed structures

Consider a set of (n -1) immersed solids S_i, with S_n corresponding to the containment, and a rigid-body acceleration (γ) of such a system. Then fluid acceleration and pressure gradient are uniform, and eq. (2) is very similar to that of hydrostatics; this implies that the resulting force on S_i is equal to ($m_{di}\gamma$), where m_{di} stands for the displaced fluid mass used in buoyancy force ($m_{di}g$). For the containment, the force is opposite, with a mass corresponding to the internal volume completely filled with fluid. Hence the consistency relationships are derived :

$$\sum_{j=1}^{n} m_{ij} = -m_{di} \qquad i = 1 \text{ to } (n-1) \tag{5a}$$

$$\sum_{j=1}^{n} m_{nj} = +m_{dn} \tag{5b}$$

Then the total sum of m_{ij}'s is equal to the fluid mass, yet this mass merely represents the fluid inertia, although the displaced masses m_{di} are typical of a fluid problem. Moreover, when considering a non-rigid but forced (or quasi-static) structural response, the relative accelerations are negligible, and the response of S_i is proportional to the loading force :

$$f_i(t) = -(m_i - m_{di})\gamma(t) \tag{6}$$

where m_i stands for the solid mass. Coupling then leads to a decrease in loading inertia forces for immersed structures, instead of a fictitious increase when allowing for a single added mass m_{ii} only. This physical interpretation of consistency relationships (5) in a particular but realistic case clearly calls for their fulfilment in coupling models.

Equations (5) are generally known for the two-body problem, i.e. "nested" bodies separated by the fluid; they have been established by Fritz (1972), and applied by Scavuzzo et al. (1979) to consistent coupling determination from the single estimate of the added mass at the inner structure (hydrodynamic mass). However, they are more often ignored for larger sets of structures, since the greater complexity requires assumptions and simplifications which may prove inadequate. A single added mass at the fuel assemblies is used in many PWR core models, neither consistent nor reflecting the in-core confinement since determined from out-of-core frequency tests. Another typical trend is to include effective coupling between neighbouring structures, but to neglect it when structures are remote or shielded by other ones. This may be quite acceptable for coupling between the immersed structures, certainly not with the containment whose acceleration generates a non-negligible pressure gradient everywhere inside.

2.4. Finite element solution and input in structural models

A finite element (f.e.) determination of the added mass matrix for coupling between rigid outlines has been described by Levy and Wilkinson (1975), but has not been found available in standard f.e. programs, where coupling is defined for deformable structures. Yet this method can easily be derived from the mathematically equivalent and widely used thermal formulation. When representing pressure by temperature, acceleration by the heat flux, the fluid matrix H to be solved is identical to the thermal one with conductivity $k = 1/\rho$. The loading vectors Q discretizing the unit acceleration of the different structures are defined such that $Q^T P$ represents the resultant of pressure forces. Hence :

$$m_{ij} = Q_i^T H^{-1} Q_j \tag{7}$$

whose perfectly symmetric feature is typical of the coupling variational formulations.

This method is implemented in the f.e. program SYSNUKE, designed for thermo-mechanical calculations in the nuclear industry. The determination of the complete two-dimensional coupling is possible, including the cross-directional XY terms. Graphical interactive facilities allow easy modelling, and the visualization of the fluid acceleration field (much more convenient than iso-pressure lines) is directly feasible since already available for the heat flux. Quadratic elements are well suited for representing the rod circular outlines and permit a relatively coarse meshing, as verified from comparison with the analytical solution for co-axial cylinders.

The plane coupling f.e. models yield values per unit height, and in the structural models, coupling is considered only between nodes at the same vertical level; the values are proportional to the modelled height (similarly to the structural mass of beams), and input in the elements coupling two nodes.

2.5. Dimensionless coefficients

Except when comparing with the structural mass, all the numerical values given hereafter are in the commonly used dimensionless form, as the ratio of the coupling term to the displaced fluid mass. This implies a right hand side equal to -1 in eq. (5a) for the immersed structures. For sets of identical structures, there is a single reference mass, and comparison is possible between all the coupling terms, except for the added mass at the containment (not considered here since the containment motion is assumed to be an input). For fuel assemblies, direct comparison is possible between different rod array sizes, including a single rod.

3. BASIC MODEL FOR A FUEL ASSEMBLY ROW

3.1. Lateral confinement hypothesis and resulting fluid models

PWR fuel assemblies are tall and laterally flexible structures only restrained at their ends by the horizontal core plates. Horizontal seismic loads then produce fuel assembly lateral distortions, and impacts between the latter or with the core vertical baffles; such impacts are located at the grids restraining the fuel rods. The current models used for the justification of fuel assembly lateral strength comprise a fuel assembly single row, excited in its own direction X, in which the assemblies are represented by beams, and springs with gaps for impacts (Callens et al., 1991).

The implicitly assumed mechanical independence of such rows can be extended to coupling by considering that the modelled row is laterally confined. Also assuming negligible gaps between rows, it has been demonstrated by Rigaudeau et al. (1993) that the lateral confinement is equivalent to identical motions of the rows and also that coupling can be determined in a fuel rod single row, parallel to the motion direction X. In the previous reference, the fluid model represents 3 "assemblies", each comprising 3 fuel rods, then allowing for inner or edge positions of assemblies and rods; in-row gaps between assemblies and with the baffles are included.

3.2. Coupling features

The coupling features corresponding to the lateral confinement are the following :

- coupling between assemblies is negligible,
- the remaining terms, i.e. the added mass m_a at assembly (hydrodynamic mass) and the coupling term m_c with the core baffles, are independent of assembly position,
- the fuel rod contributions to coupling are almost identical, which allows easy extrapolation to a full-scale rod bundle.

The numerical results from the rod single row model are given in table 1, for the 17 x 17 rod array design in which the fuel rod diameter and pitch values are 9.5 mm and 12.6 mm respectively. The fulfilment of the consistency relationship by $(m_a + m_c)$ is achieved to within a -0,001 difference, corresponding to the very small negative coupling between neighbouring assemblies.

Table 1. Coupling coefficients from the rod single row model

	Ratio to displaced fluid mass m_d	Ratio to solid mass PWR conditions
Added mass m_a	2.675	0.253
Baffle coupling m_c	- 3.674	- 0.348
$m_a + m_c \approx m_d$	- 0.999	- 0.095

The coupling model finally reduces to a two-body one, the same for all the assemblies. Consider an immersed beam (assembly), supported and excited by the containment (core plates and baffles) with acceleration $\gamma(t)$. As the coupling linear distribution along the beam is similar to that of structural mass m, the relative lateral displacement x of a node with associated height h is given by the equation :

$$h\,(\overline{m} + \overline{m}_a)\,\ddot{x} + (\text{other terms}) = -\,h\,(\overline{m} - \overline{m}_d)\,\gamma(t) \qquad (8)$$

where over-lining refers to values per unit height and the "other terms" depend on the beam stiffness and damping properties. Therefore the loading force decrease resulting from the extension of Archimede's principle (eq. (6)) applies to the beam response even when dynamic (and obviously to the response of a mass-spring system). If the frequency reduction from added mass has a limited effect on the spectrum value for the first beam mode, predominant in linear response, then this response should also be decreased by the coupling effect. Yet for the in-core seismic behaviour of the fuel assemblies, strongly non-linear because of the many impacts, the influence of coupling can be estimated only from time-history calculations, and tests (paragraph 5.2).

The somewhat surprising features of the previous coupling model can be interpreted from fluid continuity with lateral confinement, as by Rigaudeau et al. (1993) for the rod single row, and below in the more elaborate models which are precisely designed for an analytical estimate of the hypothesis validity.

4. FUEL ASSEMBLY ARRAY ANALYSIS

4.1. Model description

Figure 1 represents the fluid mesh of a 3 x 3 array of 9 x 9 rod array assemblies, reduced to one quarter from symmetries and then comprising 9000 nodes. As in section 3, the rod diameter and pitch correspond to the 17 x 17 design; the 2 mm value of gaps between assemblies or with baffles is the average in-core value. The single X direction of assembly motions is considered, to which relative positions are referred : "axial" in the X direction, "lateral" in the perpendicular Y direction.

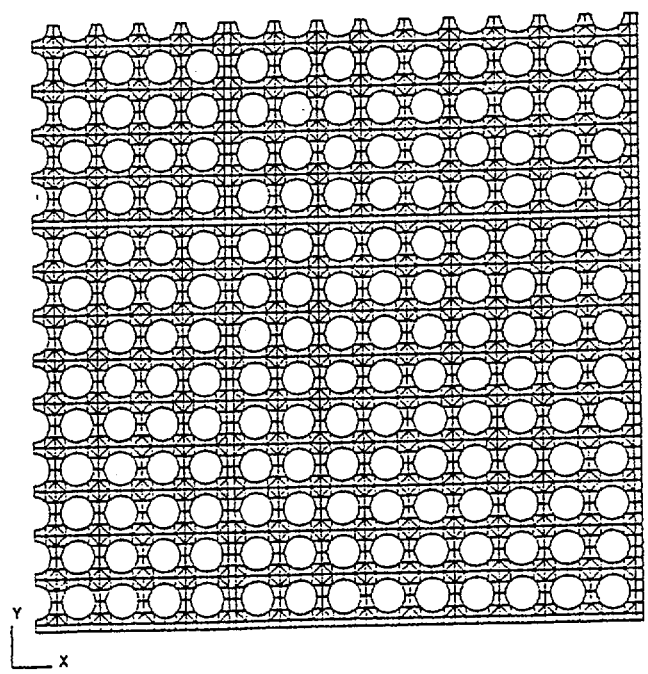

Figure 1 : Fluid model of the 3 x 3 assembly array

The motion field is skew-symmetric with respect to the symmetry axis along Y, which is represented by the boundary condition P = 0 on this axis. It is noteworthy that with the symmetry reduction, the acceleration of a single structure is possible only if the structure contains both symmetry axes (center assembly or baffles); otherwise, the non-represented symmetric structure(s) is (are) also accelerated. A complementary model of a single 9 x 9 assembly (one quarter from symmetries) allows the specific influence of lateral gaps to be studied, from zero to 35 mm values, with a 35 mm axial gap.

4.2. Restriction to identical assembly row motions

From the symmetry properties, the acceleration of all the middle assemblies in rows along X is performed, thus corresponding to identical motions of such rows. Baffles are also accelerated for a check and the acceleration visualization. Table 2 displays the m_a and m_c values for the accelerated assemblies, and when obtained from the single assembly model. Without lateral gap in the single assembly model, the values are very close to those in table 1, which are therefore confirmed for a strict lateral confinement. In the other cases, the influence of the small lateral gaps is also small but not completely negligible, thus illustrating the result sensitiveness to the lateral confinement conditions.

The fulfilment of the consistency relationship by (m_a + m_c) is (evidently) rigorous for the single assembly; in the assembly array, the differences still reflect the negligible axial coupling between assemblies, although larger than in the rod single row model because of the lateral gaps.

Table 2 : Coupling coefficients from the single assembly model and from the assembly array model.

	Added mass m_a	Baffle coupling m_c	$m_a + m_c$
Single assembly, no lateral gap	2.689	- 3.689	- 1.000
Single assembly, 2 mm lateral gap	2.489	- 3.489	- 1.000
Assembly array, center position	2.563	- 3.543	- 0.980
Assembly array, flank position	2.540	- 3.535	- 0.995

The acceleration field patterns are shown on figures 2 and 3, in the center assembly and the neighbouring regions. Such patterns are related to the acceleration flux conservation, with "sources" on accelerated outlines only, and to the existence of lateral confinement.

When accelerating all the middle assemblies in rows along X, the field cannot spread outside, where there are no flux sources, and the fluid motion is located around the accelerated rods. This leads to a very weak or zero pressure gradient in other assemblies, and therefore coupling is negligible with these assemblies; but the pressure difference generated between the accelerated assembly ends is completely transferred to the baffles, at any distance. As most of the fuel rod generated flux is transferred from one rod side to the other, there results approximate independence of fuel rod cells and therefore similar fuel rod contributions. The uniform character of coupling with baffles is still more obvious for baffle acceleration : the field appears to be space-periodic, just because the fluxes at cell boundaries are identical to the flux generated on baffles. This feature is confirmed by the uniform field in gaps along X, and moreover in the large axial gap of the single assembly model (figure 4), which displays the negligible influence of axial gaps in laterally confined models.

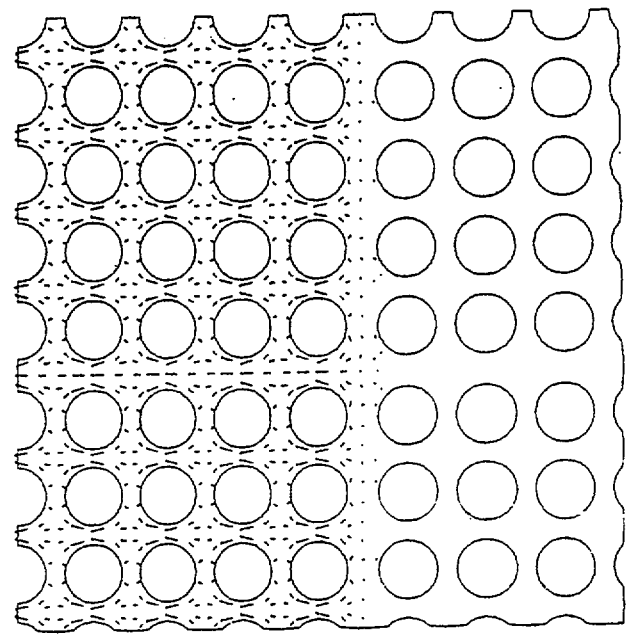

Figure 2 : Acceleration of middle assemblies in array

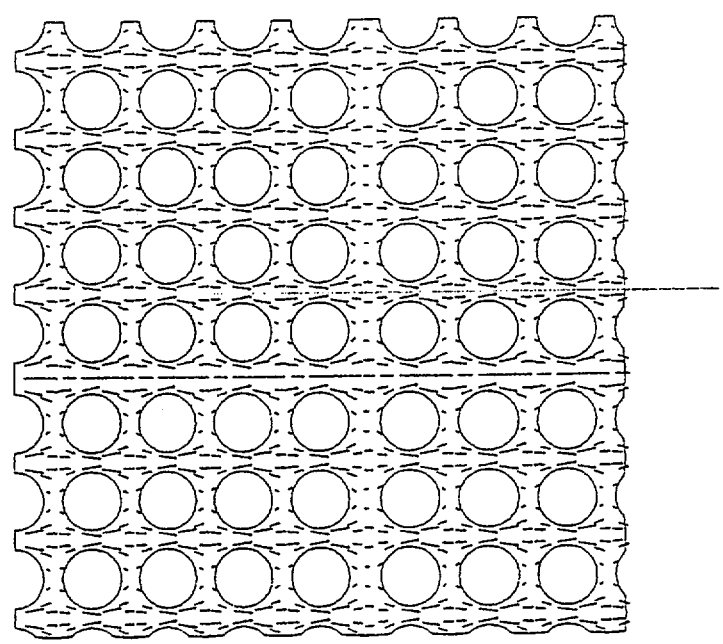

Figure 3 : Baffle acceleration in assembly array

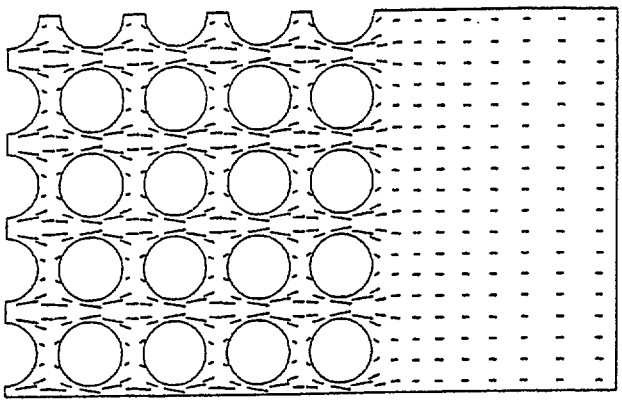

Figure 4 : Baffle acceleration in single assembly model

The approximate independence of the rod cells is confirmed by a single rod model, with baffles at cell boundaries, which yields coupling terms larger than the previous ones (without lateral gaps) by less than 10 %. It is noticeable that this property is obtained for a relatively small pitch/diameter ratio, therefore a dense array, since it is obvious only for tiny rods in wide cells, with much smaller coupling ($m_a = 1$ and $m_c = -2$ for cylinders in a large plenum). This provides a justification for the homogenization methods such as described by Brochard and Hammami (1991), which are also particularly suited to the large but confined tube bundles in steam generators.

4.3. Coupling distribution for any motion

Acceleration of the center assembly provides all the coupling terms relating to this assembly. For a more visual representation, table 3 displays the results in a geometrical configuration reproducing that of the complete 3 x 3 array, with baffles on the right : each division yields the coupling between the corresponding assembly (or baffles) and the center one, whose added mass is in the center division (1.608).

Coupling with baffles is identical to that in table 2 for the same center assembly since it may represent just as well the forces exerted on motionless assemblies resulting from baffle acceleration. Coupling between assemblies appears to be very moderate, in particular with diagonal positions, or even with axial positions and therefore in the rows along X used in seismic calculations. The more notable reduction in added mass is directly related to the larger lateral coupling terms, since from coupling linearity and symmetry, addition with these terms (sum in the table middle column) leads to the former 2.563 value.

Table 3 : Geometrical representation of coupling coefficients with the center assembly, in the assembly array.

0.093	0.477	0.093	
- 0.196	1.608	- 0.196	- 3.543
0.093	0.477	0.093	(baffles)

Without lateral confinement of the accelerated assembly, the acceleration field can spread outside (figure 5) with a pattern comparable to that in the single assembly model with a 35 mm lateral gap, for which the added mass is 1.515. The field decrease with distance, from flux conservation, is such that inter-assembly coupling remains moderate. Inside, balance with external flux requires a flux transfer and then a pressure gradient between the rod cells, opposing that around the rods and leading to the added mass decrease. The field patterns around different accelerated rods are no longer identical but remain similar, the rod added mass ranging from 1.330 to 1.936 (along the lateral and axial gap respectively), the 1.608 overall value being obtained for the central rod. Also, it is noteworthy that the assembly coupling configuration is comparable to that between individual rods. Such results are favourable to the representative character of the model size, and to the homogenization method mentioned above.

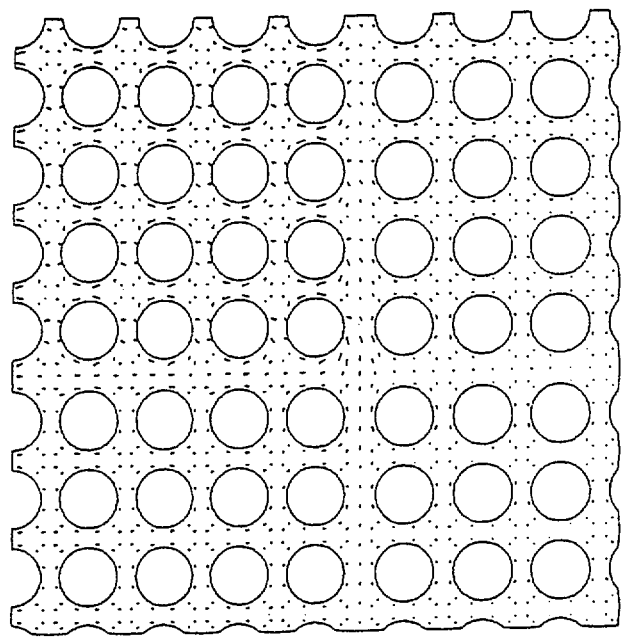

Figure 5 : Acceleration of center assembly in array

4.4. Analytical justification of the basic model

The previous results for any motion are hardly applicable to the assembly single row structural model, since the in-row coupling terms are not consistent without out-of-row coupling. Using the added mass from table 3 in the two-body basic model would lead to ($m_a + m_c$) equal to - 1.934 instead of -1, and therefore to a decrease in loading forces twice as large as the physical one. This non-conservative trend is enhanced when introducing the negative coupling terms between assemblies, which are also far too weak to have any significant influence on assembly differential motions and impacts. Neither is the development of a complete core model justified only for introducing coupling between assemblies, much smaller than with baffles.

5. FUEL ASSEMBLY SEISMIC TESTS AND CALCULATIONS

5.1. Test program

Shaker table tests on sets of interacting fuel assembly mock-ups have been undertaken in cooperation with the Commissariat à l'Energie Atomique (C.E.A.). Detailed test description and results are presented by Queval et al. (1991, 1993), and Leroux et al. (1993). The mock-ups can be arranged either in a single row (5 or 13 mock-ups) or in a reduced scale core configuration (5 mock-ups in the longest rows), with bi-axial excitation in the latter case. Tests are performed in air or in water, with a confinement simulating the core baffles, and using accelerograms generated from a seismic design basis spectrum.

The mock-up design is based on a reduced 6 x 6 fuel rod array, but with rod diameter, pitch and restraining conditions typical of the 17 x 17 design. Then the mock-up behaviour proves similar to that of a scale 1 assembly in characterization tests, i.e. single assembly lateral response without or with impacts at grid levels. The mock-up row model is built with the same procedure as for seismic analysis of scale 1 assemblies. Coupling is allowed for by the basic model previously presented, also using for comparison a single added mass at assembly, which is determined from experiments with little confinement ($m_a = 1.25$). The in-water increase in damping is found relatively small from characterization tests, and therefore should not screen the influence of coupling when introduced in the model.

5.2. Main results and consequences

For the assembly single row model representativity, one of the most important results is certainly the similar behaviour of a laterally confined row and of the longest rows in the core configuration. On figure 6, the maximum in-water impact forces, at the row ends, appear to be coherent when considering the natural scatter of such forces, which are dependent on the precise impact sequence and on the non-uniform gap distribution in the rows (gaps are uniform in the models since the actual in-core gaps are unknown). The model is found conservative, yet significantly less with the consistent coupling model than with the single added mass.

Another typical feature reflected by tests and calculations is the existence of an approximately in-phase overall motion of assemblies, between the main impact sequences which occur in assembly clusters when blocked by the baffles. As a result, coupling can be assumed as mainly exerting on a similar motion of all assemblies, which includes the basic assumption of identical row motions.

The model qualification is performed on the 13 mock-up row, in which the impact forces are larger. Figure 7 presents the in-air and in-water maximum impact forces, as an average on the 4 grids withstanding the largest forces (the two grids near mid-assembly, at both row ends). The model is still conservative, yet the consistent coupling model leads to a force decrease which is consistent with the test results, but not reflected with the single added mass. Similar trends are observed on other response parameters (force integral, number of impacts and total duration in the time-history).

Obviously, a complete and accurate validation of the coupling model is hardly feasible, due to the approximate character of the structural model, and to the complex phenomena to be described, also noting that in fuel assembly response, coupling remains a corrective term even if significant. Under such conditions, the coupling model is justified from its global coherence with the observed effects, to within

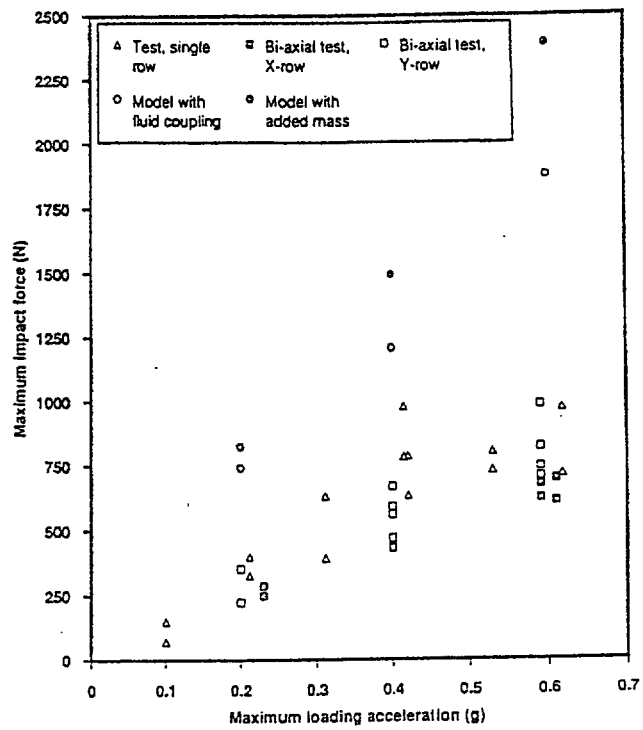

Figure 6 : Impact forces for in-water 5-mock-up rows

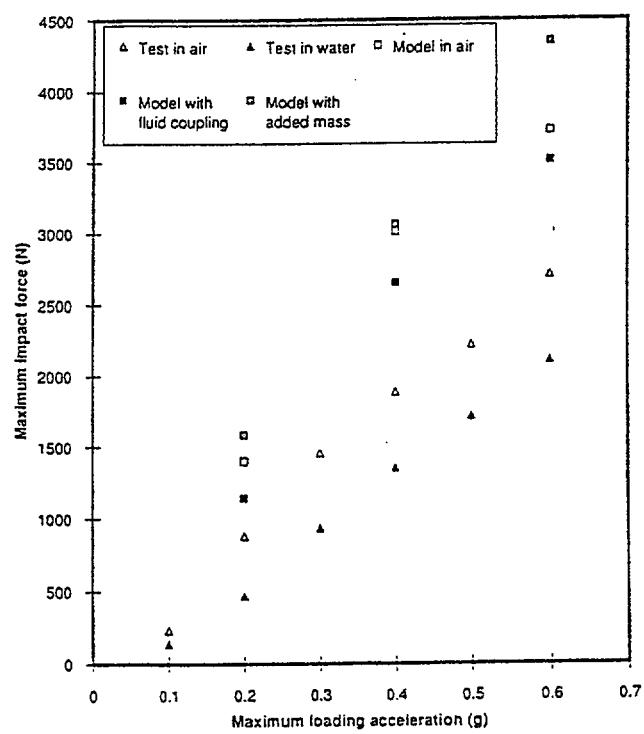

Figure 7 : Impact forces in the 13-mock-up row

e modelling uncertainties. Moreover, the model conservatism is mainly related to the impact description, much more difficult than that of assembly lateral deformations; this means that a conservatism margin reduction from the impact modelling can be envisaged only with caution, which precisely implies the elimination of clearly identified conservatisms from non-consistent coupling models.

6. FUEL STORAGE RACKS

6.1. Configuration and fluid modelling

PWR spent fuel storage racks consist of an array of rectangular modules, free-standing in a pool and comprising cells in which the fuel assemblies are inserted. The fluid mesh on figure 8 corresponds to the layout of a configuration which is simple but sufficiently representative for illustrating most of the coupling properties. The single X direction of rack motions is considered, along the longest 3-rack rows, for coupling between racks or with the pool walls only. The basic model for in-core coupling is obviously applicable to the fuel-to-cell coupling but allowing for slightly larger gaps.

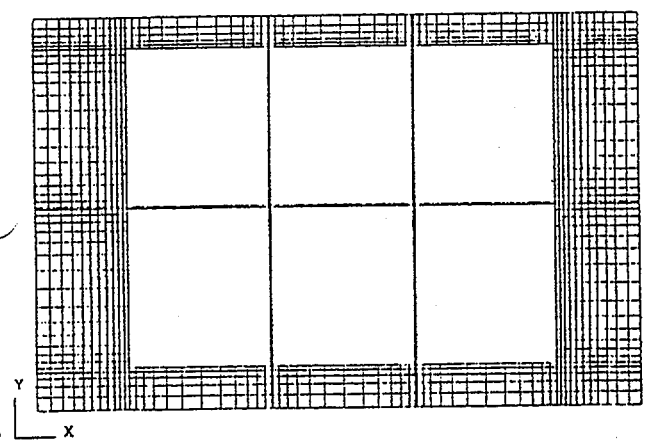

Figure 8 : Fluid model of racks in the pool

The horizontal dimensions are 12.6 m x 8 m for the pool, 2.96 m x 3.24 m for the racks, with a 34 mm gap between racks. The rack array off-centering in the Y direction is 110 mm which is little significant in coupling values. The results are given only for coupling with racks located in the row neighbouring the smaller gap with pool wall.

As the total water depth is 12 m, and the rack height is 4.43 m, the depth over the racks is large enough for neglecting the interaction with sloshing, also considering that the first sloshing frequencies are extremely small (0.25 Hz along X). However, due to the existence of the large water plenum, together with racks less slender than fuel assemblies, the coupling reduction from the vertical fluid motion is not negligible and will be briefly discussed.

6.2. Result analysis

Table 4 displays the coupling terms with the same geometrical representation as in table 3, for coupling with a reference rack either in dge (4a) or middle (4b) position in the row. The added mass at the reference rack is underlined, thus locating its position in the table. Coupling is found very large between racks, even when belonging to different rows, which is related to the relatively small gaps between opaque structures (a similar situation is encountered in fast breeder reactors, for the canned fuel assemblies). Coupling with the pool walls is notably smaller, because of the larger gaps around the rack array, yet remains essential for an appropriate description of the overall in-phase motion. The rack-to-wall coupling values are not very dependent upon rack position, as it could be expected from the general interpretation of coupling with the containment in section 2.

Table 4 : Geometrical representation of coupling coefficients with a given rack.

18.74	- 13.79	- 1.84	- 6.57	(4a)
8.36	- 4.45	- 1.46	(walls)	
- 13.79	30.10	- 13.79	- 5.75	(4b)
- 4.44	11.09	- 4.44	(walls)	

The cross-directional (XY) coupling is not intrinsically negligible, with a maximum value equal to 8.2. But the sum of the terms for a rack is zero, because this coupling has no influence in the rigid-body motion of the whole system. From symmetry considerations, this remains valid in the in-phase motion of the rack array (with negligible off-centering), or for a standard inner position of a rack in a larger array. The elimination of such a coupling is not of much importance, except perhaps for very local effects.

6.3. Remarks on practical determination and application

Many structural models comprise a rack single row (Champomier et al. 1989, Shah et al. 1994). As for fuel assemblies, the direct input of the previous values is not consistent : the sum of terms in the first rows of tables 4a and 4b, including the wall division, is equal to -3.46 or -3.23 instead of -1. Assuming identical row motions leads to the addition of the terms in the same table column (i.e. lump with out-of-row coupling) but the resulting increase in coupling terms may be found arbitrary. An alternative method is to perform a correction on the computed values (except for wall coupling), relatively weak with respect to the large values, and also required when limiting coupling to neighbouring racks. For larger arrays, the case of inner and outer rows should be distinguished. Structural models of the complete rack array are more favourable for coupling consistency, but with a complex configuration of the node-to-node coupling elements; a direct input of the total added mass matrix is certainly preferable, as when coupling is defined for deformable structures.

Allowance for the fluid vertical motion from the very large three-dimensional f.e. models is hardly feasible, and an approximate correction is acceptable. For preserving the benefit of f.e. determinations, a semi-analytical method can be envisaged : Fourier series represent the dependence on vertical position, which leads to one plane f.e. solution per included term.

7. NON-LINEAR EFFECTS

The linear character of hydrodynamic coupling is related to the hypothesis of small motion amplitudes, then leading to a negligible convective term in momentum equation (2). The general form of non-linear coupling can be derived from Lagrange equations, with an added mass matrix depending on displacements in the fluid kinetic energy. Hence the hydrodynamic force corresponding to the ith. structural degree of freedom is :

$$f_i = -\sum_{j=1}^{n} m_{ij}\ddot{x}_j - \sum_{j,k=1}^{n} a_{ijk}\,\dot{x}_j\,\dot{x}_k \qquad (9)$$

$$a_{ijk} = \frac{\partial m_{ik}}{\partial x_j} - \frac{1}{2}\frac{\partial m_{jk}}{\partial x_i}$$

where the dependence of added mass coefficients on the instantaneous geometrical configuration also implies the existence of the (non-dissipative) quadratic velocity terms.

The amplitudes of the fuel assembly lateral motions can reach values exceeding the fuel rod diameter, with resulting flows and dissipative drags, but hydrodynamic coupling is concerned only with the configuration of the rod rigid array surroundings. The influence of the configuration change is negligible with lateral confinement, since coupling is independent of the axial gaps. For the actual in-core configuration, the change in lateral gaps is more significant, but its influence is likely to have the same order of magnitude as the neglected coupling between assemblies, and to be negligible in the key coupling with baffles. Linearity is therefore consistent and justified with the basic model.

Non-linear phenomena occur in the fluid layers between assembly grids (including dissipative), related to the squeeze film dynamics described by Esmonde et al. (1992). Yet the total height of the grids is relatively small (10 % of assembly), and coupling effects between grids cannot be clearly identified from the seismic tests in section 5.

A significant coupling non-linearity is a priori more obvious in the large coupling between racks, and practical forms of eq. (9) have been established from approximate macroscopic balances by Stabel et al. (1993). The method is attractive, but the coupling influence should be compared with that from linear models, which are easier to handle and also reflect a large response decrease in water. It is believed that the model refinement brought by non-linearity should be balanced with the many approximations in the structural models and in coupling distribution, in a reasonable estimate of the predominant phenomena in seismic response.

8. CONCLUSIONS

Hydrodynamic coupling is characterized by very simple governing equations and representation in structural models, yet this simplicity may be misleading for coupling interpretation and determination. For large sets of immersed structures, the necessary simplifications should lead to a physically consistent behaviour in the limiting cases of in-phase motions, and coupling with the containment is never negligible. For the fuel assembly single row models currently used in seismic analysis, assuming row lateral confinement reduces coupling to that between assembly and core baffles, independent of assembly position. This very simple coupling model is justified from the small coupling between assemblies found with calculations, and from its coherence with the in-water response decrease observed in seismic tests; the tests also justify the single row model. Then the artificial conservatism of the models comprising a single added mass at assembly is eliminated. The large coupling between fuel storage racks is more complex to analyze and to implement. A careful estimate of the different approximations is recommended, in relationship with the computed or tested seismic response, in order to preclude illusory sophistications in structural or coupling models. It is hoped that apart from practical results, the previous considerations will provide useful guidelines for appropriate modelling of coupling, more especially since complete and accurate experimental validations are hardly feasible.

REFERENCES

Brochard D., Hammami L., 1991, Non-Linear Seismic Analysis of Nuclear Reactor Cores by an Homogeneization Method, PVP Conf., San Diego, Vol. 223.

Champomier F., Delemontey R., Sollogoub P., Toumbas D., 1989, Seismic Design of a Spent Fuel Storage Rack, SMIRT 10, Anaheim, Vol. K 2.

Callens C., Leroux J.C., Rigaudeau J., 1991, Status of Methods for Justification of Fuel Assembly Lateral Strength during an Earthquake, SMIRT 11, Tokyo, C 6/1.

Esmonde H., Fitzpatrick J.A., Rice H.J., Axisa F., 1992, Modelling and Identification of Non-linear Squeeze Film Dynamics, Jour. of Fluids and Structures, 6, 223-248.

Fritz R.J., 1972, The Effects of Liquids on the Dynamic Motions of Immersed Solids, ASME Jour. of Engin. for Industry, 94, 167-173.

Jeanpierre F., Gibert R.J., Hoffman A., Livolant M., 1979, Description of a General Method to Compute the Fluid Structure Interaction, SMIRT 5, Berlin.

Leroux J.C., De Perthuis S., Rigaudeau J., 1993, Qualification of Industrial Models for the Justification of Fuel Assembly Lateral Strength during an Earthquake, SMIRT 12, Stuttgart, K 16/1.

Levy S., Wilkinson P.D., 1975, Calculation of Added Water Mass Effects for Reactor System Components, SMIRT 3, London, F 2/5.

Rigaudeau J., Brochard D., Benjedidia A., 1993, Fluid Structure Interaction in the Response of PWR Fuel Assemblies to Horizontal Seismic Loads, SMIRT 12, Stuttgart, K 17/5.

Queval J.C., Gantenbein F. , Rigaudeau J., 1991, Experimental Studies on Seismic Behaviour of PWR Fuel Assembly Rows, PVP Conf., San Diego, Vol. 20.

Queval J.C., Gantenbein F., De Perthuis S., 1993, Experimental Studies on Seismic Behaviour of PWR Fuel Assemblies, SMIRT 12, Stuttgart, 17/6.

Scavuzzo R.J., Stokey W.F., Radke E.F., 1979, Dynamic Fluid Structure Coupling of Rectangular Modules in Rectangular Pools, PVP 39, 77-86.

Shah S.J., Harstead G.A., Kopecky B., 1994, Seismic and Structural Analysis of High Density/Consolidated Spent Fuel Storage Racks, ANS meeting, DOE Spent Nuclear Fuel - Challenges and Initiatives, Sun Valley.

Stabel J., Ren M., Swelim H., 1993, Calculation of Seismic Loads on Fuel Storage Racks under Consideration of Fluid Structure Interaction, SMIRT 12, Stuttgart, K 15/6.

ADDENDUM 2 TO BAW-10133-A, Rev.1
Mark-C Fuel Assembly
LOCA-Seismic Analyses

Framatome Cogema Fuels
P.O. Box 10935
3315 Old Forest Drive
Lynchburg, Va. 24506-0935

ABSTRACT

The justification of the PWR fuel assembly strength under seismic and LOCA loads is performed by means of assembly row models described in Reference 1. The resulting response magnitudes are greatly dependent on the damping input in the fuel assembly model.

Currently the limit on structural damping under axial flow at reactor operating conditions for the seismic and LOCA loads reported in the previous report (Reference 1) is [b, c, d]. The existence of a large damping increase under axial flow is clearly demonstrated by test results. Hydraulic testing under reactor operating conditions has demonstrated damping values in excess of [b, c, d] in several fuel assemblies mechanical test programs performed in hydraulic loops. The object of this addendum is to propose and justify higher damping values in fuel assembly seismic and LOCA models as this will contribute to promote optimized products, which will produce conservative margins.

TABLE OF CONTENTS

Page

1.0 INTRODUCTION 1-1

2.0 APPARATUS 2-1

2.1 FCF Test Facilities 2-1
2.2.1 Control Rod Drive Line (CRDL) Facility 2-1
2.2.2 Fuel Assembly Mechanical Evaluation (FAME) Facility 2-1
2.2 Framatome Test Facility 2-2
2.2.1 Hermes-T Loop Test Facility 2-2

3.0 FUEL ASSEMBLY 3-1

3.1 FCF Fuel Assembly 3-1
3.2 Framatome Fuel Assemblies 3-1

4.0 HOT FLOW TESTS 4-1

5.0 TEST RESULTS 5-1

5.1 Frequency 5-1
5.1.1 FCF Test Results 5-1
5.2 Damping 5-1
5.2.1 FCF Test Results 5-1
5.2.2 Framatome Test Results 5-2

6.0 APPLICATION OF TEST RESULTS FOR HIGHER MODES 6-1

7.0 CONCLUSIONS 7-1

8.0 REFERENCES 8-1

Appendix A - Response to NRC Question A-1

List of Figures

Figure

2-1 Control Rod Drive Line (CRDL) Facility 2-3
2-2 FAME Facility 2-4
2-3 Hermes-T Test Section 2-5
5-1 FCF Mark-C 17x17 FA – Effect of Temperature on Frequency 5-3
5-2 FCF Mark-C 17x17 FA – Frequency Response 5-4

Page

5-3 First Natural Frequency versus Effective Amplitude of Displacement ... 5-5
5-4 FCF Mark-C 17x17 FA – Effect of Temperature on Damping 5-6
5.5 FCF Mark-C 17x17 FA Average First Cycle Damping Under Flowing Conditions 5-7
5.6 Damping versus Effective Amplitude of Displacement 5-8

1.0 INTRODUCTION

In accident conditions (seismic and LOCA), the damping of fuel assemblies in their lateral deformation response is increased significantly by the axial flow of the primary coolant. Currently, the limit on structural damping under axial flow at reactor operating temperature conditions for seismic and LOCA load calculations reported in the previous report (Reference 1) is [b, c, d]. Hydraulic testing under reactor hydraulic operating conditions has demonstrated damping values in excess of [b, c, d] in several fuel assembly mechanical test programs performed in hydraulic loops. The object of this addendum is to propose and justify higher damping values to be used in accident analyses.

FCF and Framatome have performed tests on fuel assemblies in water under both cold and hot water conditions. The first FCF hot-flow in-loop tests performed with a Mark-C 17x17 fuel assembly were described in Reference 2. From this test, the effect of flowing water on the damping of the fuel assembly is presented. Other data obtained in the Framatome Test Program using similar fuel designs are also presented to show the presence of the large damping values under axial flow. Framatome test results have been presented in References 3 and 4. Several fuel design configurations were used in the Framatome test programs.

The test results are presented for the primary mode since it is usually measured in the hydraulic-loop tests and it is predominant in the fuel assembly seismic response.

2.0 APPARATUS

Fuel assembly damping tests were performed by both FCF and Framatome in water at conditions that simulated the complete range of reactor operating flow conditions. The experimental facilities used by FCF and Framatome for these tests are described in this section.

2.1 FCF Test Facilities

The test facilities used for FCF fuel assembly testing are described as follows:

2.1.1 Control Rod Drive Line (CRDL) Facility

This facility incorporates a 17-inch (432 mm) ID by 40-foot (12.2 m)-long pressure vessel for demonstrating capabilities of the control rod drive system and investigating fuel assembly response in an environment simulating that of a PWR (2250 psig, 635^{0}F and full fuel assembly flow). The main fuel assembly test section of the CRDL is approximately 16.7 feet (5.09 m) long.

A full size prototype fuel assembly, control rod assembly, control rod drive line, and drive mechanism and internal guide tube structure are tested as part of the fuel assembly mechanical test program. The fuel assembly is restrained in the CRDL autoclave by grid pads simulating the reactor internals interface. Coolant flow is directed through flow channels above, below, and around the fuel assembly to simulate the flow distribution around a single fuel assembly in the reactor.

A schematic of the CRDL facility is shown in Figure 2-1.

2.1.2 Fuel Assembly Mechanical Evaluation (FAME) Facility

This facility is used to provide information about the dynamic structural response and static behavior of fuel assemblies in air. The FAME facility consists of a rigid frame with grid pads that accurately simulate the stiffness and restraint of the reactor internals' interface with the fuel assembly upper and lower end fittings. A schematic of the FAME facilty is shown in Figure 2-2.

Additionally, this facility includes an electrodynamic shaker system capable of producing harmonic sinusoidal frequencies from 1 Hz to 200 Hz with associated instrumentation.

A full size prototype assembly is tested in this facility to determine the basic fuel assembly static and dynamic structural characteristics.

2.2 Framatome Test Facility

The test facility used for Framatome fuel assembly testing is described below.

2.2.1 Hermes-T Test Loop Facility

The facility is located at the 'centre nucleaire de Cadarache" in France. The Hermes installation is an experimental complex that can reproduce the conditions of a pressurized water reactor (pressure, temperature and flow conditions). This loop is designed to flow test PWR full scale fuel assemblies as well as their associated control components. The main fuel assembly test section of this closed loop consists of a 460 mm (18.1 in.) inside diameter, 5.2 m (16.9 ft.) long pressure vessel capable of withstanding the pressure and temperature conditions. Inside this pressure vessel is the holding basket. This basket, which constitutes a hydraulic pipe, can have different geometries, depending on the type of assembly to be tested. The lower part of the basket simulates the lower core support plate. The upper part simulates the upper core support plate against which the fuel assembly holddown springs press. Any type of PWR full-scale fuel assembly can be tested in this facility with appropriate modifications.

The Hermes-T test loop is shown in Figure 2-3.

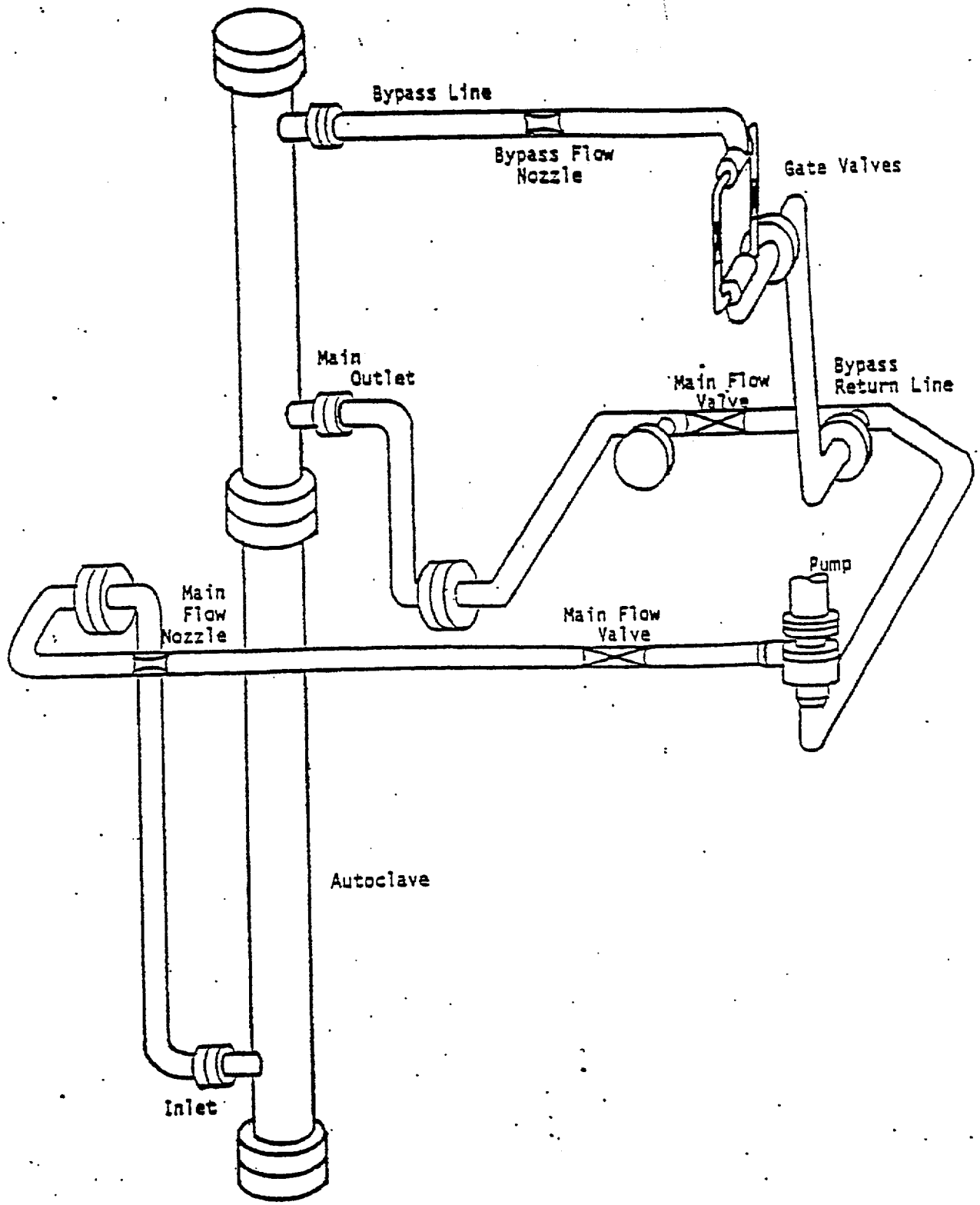

Figure 2-1 Control Rod Drive Line (CRDL) Facility

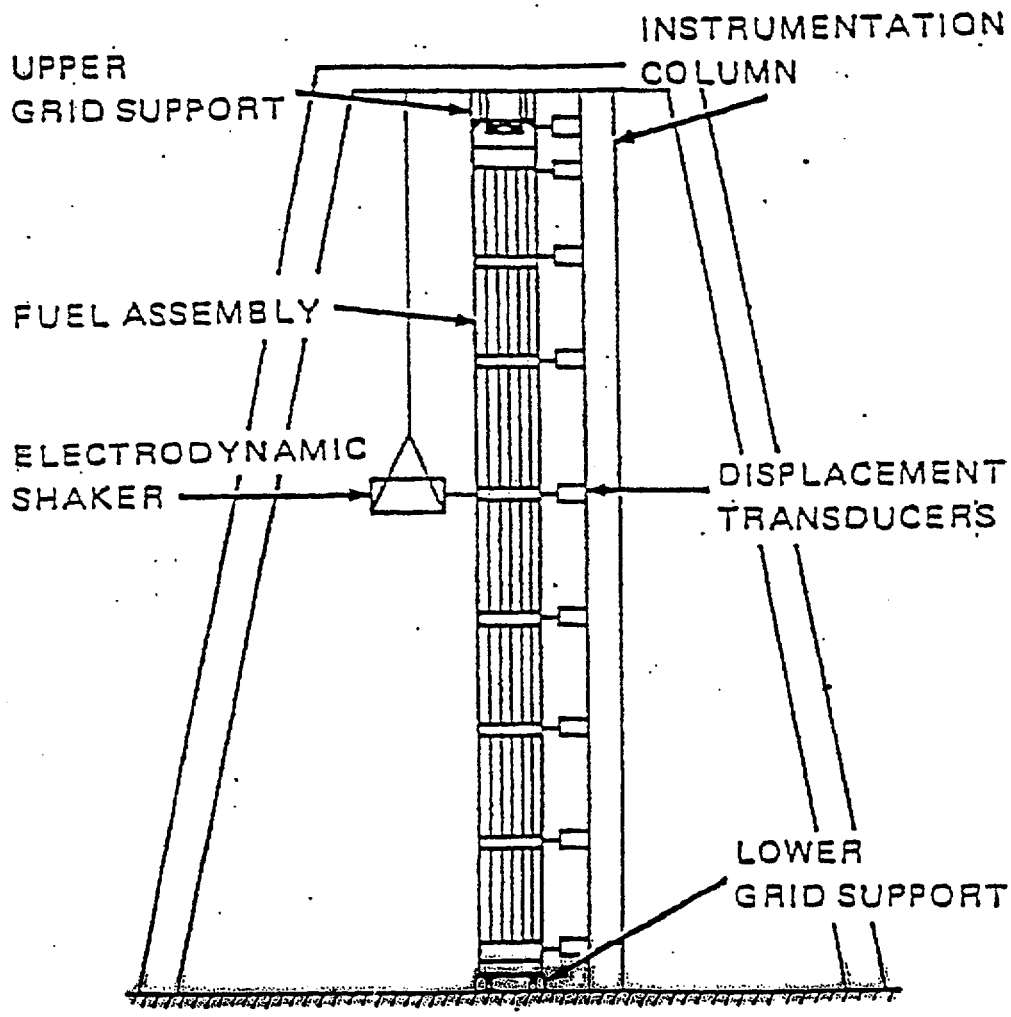

Figure 2-2 FAME Facility

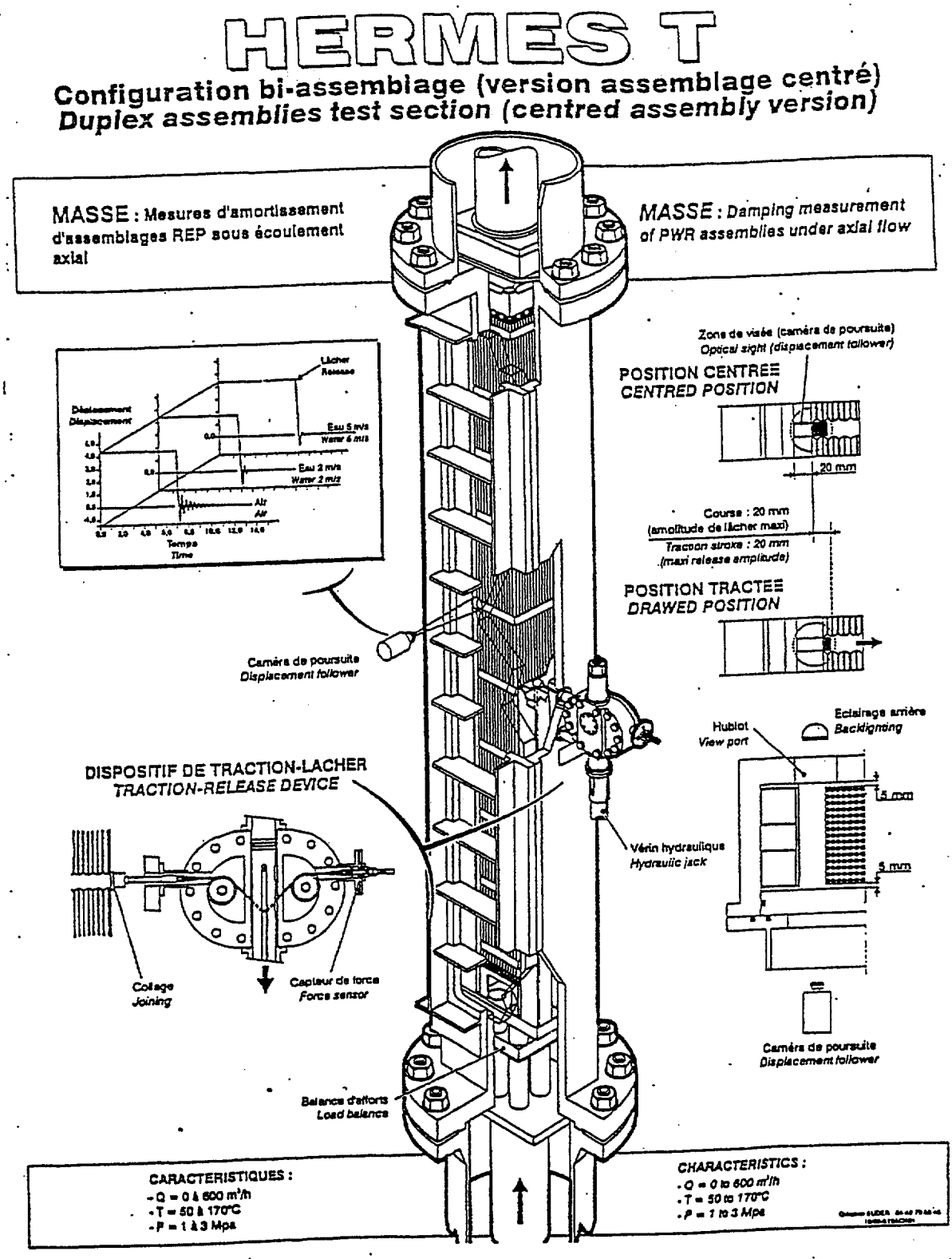

Figure 2-3 Hermes T Section

FRAMATOME COGEMA FUELS

3.0 FUEL ASSEMBLY

3.1 FCF Fuel Assembly

The prototype fuel assembly tested by FCF featured a 17x17 array with 264 fuel rods, 24 control rod guide tubes, and one instrument tube. The overall dimensions of the prototype corresponded to a full scale Mark-C fuel assembly, which is described in Reference 2. Span lengths were similar to those of full-scale fuel assemblies.

3.2 Framatome Fuel Assemblies

Two prototype fuel assemblies were utilized in the test program. One assembly featured an 8x8 array with 4 guide-thimbles, 5 spacer grids, and a 1.9 m height between the fuel assembly nozzles. The overall dimensions roughly corresponded to ½ scale. The fuel rod diameter and pitch were identical to the overall structure of a PWR fuel assembly. Span lengths were similar to those of full-scale assemblies. The other assembly featured a full-scale Framatome 17x17 array fuel design.

4.0 HOT FLOW TESTS

FCF performed fuel assembly hot flow tests in the CRDL facility over the entire operating spectrum of a pressurized water reactor. Impulse tests, similar to those carried out in air, were performed. The primary purposes of the impulse test were:

1. To provide the fundamental frequency and damping of the fuel assembly under the influence of water for use in the fuel assembly dynamic analysis.

2. To verify the predicted response.

Lateral deflection of the fuel assembly was provided by a hydraulic plucking mechanism. Actuation of a solenoid valve resulted in rapid release of the pressure supplied to the plucking device. This moved the device away from the bundle and permitted free vibration of the assembly. Fuel assembly motion was traced by a Linear Displacement Transducer (LVDT) positioned at the third intermediate grid from the bottom. At each test condition, the fuel assembly was deflected approximately 3.6 mm, then released and allowed to vibrate freely. The response of the assembly, in the form of time-displacement history, was monitored on-site and recorded on tape for analysis.

A Hewlett Packard Fourier Analyzer was used to reduce the majority of the data. The amplitude and time position of each peak was determined. A zero line through the data is obtained by averaging an even number of positive and negative peaks. All amplitude values are referenced to this zero line.

The percent critical damping was calculated, assuming a single degree of freedom viscously damped structure, using the following formula.

$$\% \text{ critical damping} = \frac{100\delta}{(\delta^2 + 4\pi^2)^{1/2}}$$

where the logrithmic decrement for the positive peak is:

$$\delta = \ln \frac{A_i}{A_{i+2}}$$

where i=1,2,3 ..

A_i = amplitude of first cycle positive peak
A_{i+2} = amplitude of next cycle positive peak
δ = logrithmic decrement

The frequency for the particular cycle of interest is the reciprocal of the time between peaks:

$$f = \frac{1}{t_{i+2} - t_i}$$

where i =1,2,3 ..

t_i = time at first cycle

t_{i+2} = time one cycle later

The time history plots obtained were sinusoidal curves of decaying amplitude. High damping of the fuel assembly caused by the virtual mass of the water resulted in vibration amplitudes less than 2.0 mm. Initial displacements were approximately 3.6 mm.

Framatome has performed several test programs in hydraulic loops using fuel assembly prototypes with a rod lattice of 8x8 and a rod lattice of 17x17. Damping calculations on these prototypes were performed by the logarithmic decrement method on free oscillations, from the equation shown above. Test conditions were in air and in water with flow velocities from 0 to 5 m/s (0 to 16.4 ft/s), at room temperature. An oscillatory motion confinement range of 5 to 65 mm was used.

5.0 TEST RESULTS

Frequency and damping information were obtained for each of the FCF and Framatome tests. The results presented below are a summary of the test outputs. FCF and Framatome in-water pluck tests were conducted in several confinements, with basically the following differences.

- FCF tests were performed at reactor temperature, but at relatively small initial displacement amplitudes.

- Framatome tests were conducted with large displacement amplitudes and various confinement conditions but mostly limited to room temperature. A test at 170^{0}C (338^{0}F) confirmed the results of the FCF tests which showed that the influence of temperature on the damping value is insignificant.

5.1 Frequency

5.1.1 FCF Test Results

The average frequency response of the fuel assembly versus amplitude for a range of temperatures at zero flow is plotted in Figure 5-1. The temperature of the environment and the resulting change in density and viscosity have no apparent effect on fuel assembly frequency. Figure 5-1 also provides a comparison of the response of the prototype assembly in the CRDL and FAME facilities. The fuel assembly frequency in the CRDL facility falls within the lower bounds of that obtained in the FAME facility. Figure 5-2 shows the frequency response of the fuel assembly as a function of amplitude at a temperature of 600^{0}F and a flow rate of 500 gpm (corresponding to a flow velocity of 4.2 ft/s). The frequency response at flow conditions is the same as at zero flow. The change from an air to water environment decreased the frequency by approximately [b, c, d] percent, due to added hydraulic mass of the water.

5.1.2 FramatomeTest Results

Figure 5-3 displays the results of the first natural frequency obtained in air and in water with the Framatome 8x8 and the 17x17 fuel assembly mock-ups. In both cases, the frequency decreases when amplitude increases because of non-linear behavior due to rod slippage in grid cells. Framatome tests also indicate a decrease in the frequency for in-water tests with respect to in-air tests due to the added mass effect.

5.2 Damping

5.2.1 FCF Test Results

The in-air damping of the fuel assembly in the CRDL and FAME facilities is shown in Figure 5-4. The good agreement between the in-air data from both the CRDL and FAME facilities suggests that the end fixity of the fuel assembly may be assumed to be the same

in both the facilities. This is of significant importance, since data from both facilities can be used together in the dynamic analysis of the fuel assembly.

Comparison of in-air and in-water results indicates an increase of nearly [b, c, d] percent in damping, due to the increased density of water. Figure 5-4 also provides the percent critical damping versus amplitude as a function of temperature at zero flow. The damping of the fuel assembly and the response frequency appear to be independent of the water temperature. This was observed in vibration tests of other fuel assembly designs also. This implies that water density and viscosity have little effect on damping for the temperature conditions evaluated.

Introduction of axial flow contributes significantly to the damping of the fuel assembly as shown in Figure 5-5. The percent critical damping ranged from [b, c, d to b, c, d] over the range of test flow rates 0 to 2500 gpm (which correspond to the range of flow velocities 0 to 21 ft/s (0 to 6.40 m/s)). These results show a [b, c, d] increase in damping due to due to the coolant flow as compared to zero flow.

5.2.2 Framatome Test Results

For the Framatome 8x8 and 17x17 fuel assembly mock-ups, the results of damping versus flow rates and amplitudes of displacement are presented in Figure 5-6. It shows the results of damping in air, with no flow, and with axial flow rates between 3 m/s and 5 m/s (9.8 ft/s to 16.4 ft/s).

For the axial flow velocity range of 0 m/s to 3 m/s (9.8 ft/s), the relative increase in damping shown in Figure 5-6 is about [b, c, d] for the 8x8 mock-up fuel assembly and [b, c, d] for the 17x17 mock-up fuel assembly. For axial flow rates, increasing from 0 m/s to 5 m/s (16.4 ft/s), relative increases in damping for the 8x8 mock-up fuel assembly and for the 17x17 mock-up fuel assembly are [b, c, d] and [b, c, d], respectively.

The influence of confinement in the movement direction is found to be [b, c, d] for a given axial flow rate.

From both the FCF and Framatome tests described above, the damping of the first mode is slightly larger than [b, c, d] at the in-core velocity of 16.4 ft/s (5 m/s). Therefore, the input of [b, c, d] damping value is applicable, while maintaining conservatism margin for the first mode in the fuel assembly dynamic analysis core models.

b, c, d

Figure 5-1- FCF Mark-C 17 x 17 FA
Effect Of Temperature On Frequency

b, c, d

Figure 5-2 FCF Mark-C 17 x 17 FA Frequency Response

b, c, d

Figure 5-3 First Natural Frequency Versus Effective Amplitude of Displacement

b, c, d

Figure 5-4 FCF Mark-C 17 x 17 FA
Effect Of Temperature On Damping

b, c, d

Figure 5-5 FCF Mark-C 17 x 17 FA Average First Cycle Damping Under Flowing Conditions

b, c, d

Figure 5-6 Damping Versus Effective Amplitude of Displacement

6.0 APPLICATION OF TEST RESULTS FOR HIGHER MODES

The present damping value in Reference 1 is [b, c, d] and [b, c, d] for the first and third modes respectively. For mode 3, which is minimally affected by the amplitude, a damping value that is [b, c, d] can be justified based on the fuel assembly shaker modal test results performed in air. The shaker table modal tests were performed in air at room temperature to provide the first five natural frequencies; damping at each of those frequencies; model shape for each of these frequencies; and the effect of vibration amplitude and axial load on the above characteristics. The damping values that were recorded for the prototype fuel assembly in air at room temperature at very low amplitude are as follows:

[b, c, d]

Based on the shaker table modal test results above, the first and third mode damping values are [b, c, d]. Therefore using a damping value for the third mode equal [b, c, d] is conservative. Thus, given the proposed [b, c, d] damping for the first mode, a conservative value of [b, c, d] damping for the third mode is proposed.

7.0 CONCLUSION

The FCF and Framatome test results clearly confirm the large damping values under axial flow. At the in-core velocity 5 m/s (16.4 ft/s), which is lower than design flow velocity, the dimensionless damping of the first mode is greater than [b, c, d] of critical. This observance of large damping was consistent in all of the tests. The influence of the fuel assembly configuration was not found to be significant. For a higher mode, a very conservative damping value that is [b, c, d] is found to be acceptable based on the fuel assembly shaker modal test results.

Therefore, the input of larger damping values in the fuel assembly dynamic analysis core models is justified for all FCF PWR fuel designs based on the supporting test data. Damping values beyond the [b, c, d] value currently used for the first mode are applicable. Therefore, the [b, c, d] and [b, c, d] damping values for the first mode and higher modes, respectively are conservative compared to empirical fuel assembly damping values and are proposed for use in the fuel assembly seismic and LOCA structural licensing analysis methodology.

8.0 REFERENCES

1. BAW-10133P, Rev. 1, Addendum 1, Mark-C Fuel Assembly LOCA-Seismic Analyses, September 1997.

2. BAW-10097PA, Rev. 2, Mark-C (17x17) Fuel Assembly – Research and Development- Revision 2, January 1976.

3. Fardeau, P., Barbier, D., de langre., Rigaudeau, J., "Damping from Axial Coolant Flow in the Response of PWR Fuel Assemblies to Horizontal Seismic Loads", SMIRT 14, Lyon 1997, Paper J04/4.

4. Barbier, D., Rigaudeau, J., Viallet, E., "Damping from Axial Coolant Flow in the Response of PWR Fuel Assemblies to Horizontal Seismic Loads", ICONE 6, San Diego 1998, Paper 6156.

APPENDIX A

Response to NRC Questions

RESPONSE TO NUCLEAR REGULATORY COMMISSION QUESTION ON BAW-10133P, REVISION 1, ADDENDUM 1
"MARK-C FUEL ASSEMBLY LOSS-OF-COOLANT ACCIDENT (LOCA) AND SEISMIC ANALYSIS" JULY 17, 2000

QUESTION

The March 17, 2000 response to Question 6 of the NRC's request for additional information dated January 4, 2000, mentions that "recent (November 1999) resonance tests performed at CEA in water under axial flow conditions ... " demonstrate that the damping value for higher modes used in Addendum 2 is justified. Please provide this data for the staff to verify that the damping used is valid.

RESPONSE

GENERAL DESCRIPTION AND COMMENTS

The MASSE 99 resonance tests were performed in the same loop (Hermes-T) and under similar conditions as the MASSE 96 pluck tests described in Addendum 2. A full size 17x17 fuel assembly mock-up [b,c,d] was utilized for this testing program. The MASSE 99 tests were performed in air and in water with the axial flow velocity range of [b,c,d] at temperature of [b,c,d].

Resonance test results obtained in water under axial flow conditions are provided in Figures 1 through 3 with some comments provided below.

1. Figure 1 - Damping vs. amplitude diagram for mode 1, from resonance, in air and in water with different flow velocities and amplitude up to [b,c,d].
2. Figure 2 - Damping vs. flow velocity diagram for mode 2, with [b,c,d] amplitude; flow velocity is [b,c,d]. Despite the unfavorable loading position for mode 2, a weak resonance has been obtained up to a [b,c,d] flow velocity. It is shown that this mode features a damping increase under flow, which is similar to that of mode 3, and it is very likely that their respective damping values are very similar or even higher for mode 2.
3. Figure 3 - Damping vs. amplitude diagram for mode 3, in air and in water with different flow velocities and amplitude up to [b,c,d].

b, c, d

Figure 1 Damping Measurement Under Axial Flow for Mode 1

b, c, d

Figure 2 Damping Measurement Under Axial Flow for Mode 2

b, c, d

Figure 3 Damping Measurement Under Axial Flow for Mode 3

RESPONSES TO NUCLEAR REGULATORY QUESTIONS ON BAW-10133P, REVISION 1, ADDENDUM 2
"MARK-C FUEL ASSEMBLY LOCA AND SEISMIC ANALYSIS," JULY 17, 2000

1. Regarding simulated seismic and LOCA events, how much of the impact force is attributable to the response of the higher modes compared to that of the first mode?

Response

In the seismic response, the deformed shapes are similar to that of the first mode and the impact force distributions feature a maximum at mid assembly, which shows that the first mode is notably predominant. In addition, the influence of the first mode damping is much larger than for the higher modes damping (see response to Question 7).

In the response to LOCA, the differential motion of the core plates plays a more significant role than any particular mode. The largest impact forces are located near the top of assemblies. They typically do not feature a maximum at mid assembly. In the LOCA, the damping is not important in any mode and its effect remains small because the response is a very short transient, without sustained oscillations.

The previous considerations show that the influence of damping for modes higher than 1 is small in faulted condition analysis. This is favorable to the modeling since damping determination is easier and more reliable for mode 1.

Grid forces are also dependent on the input time histories used. Thus, it is difficult to generalize what percentage of the impact force is attributable to the response of the higher modes compared to that of the first mode. For this reason based on the higher mode test results a conservative value of [b,c,d] was chosen.

2. Were the boundary conditions for the prototype assemblies tested similar to those typical of most reactor seismic and LOCA events? Please discuss any differences and the impact of these differences on seismic and LOCA analyses. Also discuss any differences in boundary conditions between beginning-of-life assemblies and end-of-life assemblies and their impact on seismic and LOCA analyses.

Response

In the test facility, the prototype fuel assembly was supported by mock core plates with guide pins to simulate the end conditions in the reactor. These constraints accurately simulate the stiffness and restraint of the reactor internals interface

with the fuel assembly upper and lower nozzles. Thus, the boundary conditions for the prototype assemblies are very similar to the restraint of the reactor internals interface.

A holddown force was applied on the prototype fuel assembly corresponding to a beginning-of-life (BOL) condition in the reactor. The fuel assembly lateral dynamic behavior is largely independent of axial load. The mechanical interactions between assembly nozzles and guide pins are not modified. Hence, differences between BOL and end-of-life (EOL) boundary conditions (increasing compressive axial load) are negligible.

3. How would the energy dissipation of assembly internals differ between irradiated fuel assemblies and the unirradiated assemblies that you tested? For example, would cracked fuel pellets and the elimination of the fuel-cladding gap influence damping? Please discuss the possible differences in damping and response between the assemblies tested and end-of-life irradiated fuel assembles for seismic and LOCA events.

Response

BOL and EOL conditions affect fuel assembly structural damping which is much smaller than flow-induced damping. The flow-induced damping dominates regardless of BOL and EOL conditions of the fuel assembly. At EOL conditions, the structural damping increases (secondary effect). The main effect of the flow induced damping is on the fuel assembly and not on the fuel rod itself. The structural damping of the fuel assembly in air can be interpreted as mainly resulting from slippage of the fuel rods through the grid cells. An increase of damping from BOL to EOL conditions will tend to reduce the maximum impact force.

4. The testing performed did not allow for any assembly-to-assembly interaction. What influence would assembly-to-assembly interaction have on damping? During seismic and LOCA events what percentage of damping is due to mechanical fuel rod and assembly interactions and what percentage is due to coolant flow?

Response

Assembly to assembly interaction (or with core baffles) corresponds either to friction or to impact at grid levels, both providing supplementary energy losses. This dissipation of energy was not considered in the analysis, which provides additional conservatism for the fuel assembly loading condition analysis. The impact model includes a specific grid damping (see Addendum 1), which is smaller and has a more limited influence than the beam damping considered in the

core model. The damping due to flow rates is so dominant that small changes in damping due to assembly to assembly mechanical interaction are over-shadowed.

According to test results, about [b,c,d] of damping can be attributed to purely structural effects, [b,c,d] to the coolant flow at nominal in-reactor velocity of [b,c,d].

5. The loading of the assemblies in the testing done at the Hermes-T Test Loop Facility consisted of releasing a prescribed displacement at approximately mid span. This type of loading will produce a response which is dominated by the odd modes of vibration (first, third, etc.). Were loading tests performed to study damping effects of even modes in water? If not, please discuss the impact of possible differences in damping between odd and even modes on assembly response during seismic and loca events.

Response

The pluck tests with pull and release near mid assembly can provide useful results for the first mode only. All the determinations relating to higher modes are performed by resonance tests. For damping under axial flow, the resonance tests performed in the Hermes-T loop are recent (end of 1999) and limited to mainly modes 1 to 3 due to specific constraints in the in-loop determination of large damping values. However, under a weak resonant condition, limited damping measurements up to a [b,c,d] flow velocity for mode 2 were taken. The fuel assembly damping for mode 2 is [b,c,d] at the flow velocity of [b,c,d] (design flow velocity [b,c,d] at amplitude of [b,c,d]. The damping values for modes 1, 2 and 3 under axial flow conditions are provided in Figures 1 through 3 respectively. These plots show that the damping for the first mode and the higher modes increases with the flow velocity. The damping is greater than [b,c,d] for a fuel assembly lateral deflection of [b,c,d] for all the modes.

6. For limiting seismic and LOCA events, how does anticipated assembly damage compare when using the previous damping values relative to the new proposed higher damping values?

Response

A comparison study was performed for the limiting seismic time history using the previous damping values relative to the new proposed damping values. For seismic response, an increase of the damping from [b,c,d] to [b,c,d] for the first frequency reduces the maximum impact force on grids by [b,c,d]. For higher mode damping, an increase from [b,c,d] to [b,c,d] leads to an impact force increase by [b,c,d]. This slight increase is insignificant and it confirms the influence of damping for modes higher than 1 is small. For the damping values of [b,c,d] for the first mode and [b,c,d] for the third mode, the maximum impact force is reduced by [b,c,d].

A similar study was performed for LOCA response. The influence of the variations in damping considered in this study is very small for the LOCA response. It caused only minor reduction in impact loads (not greater than [b,c,d] reduction in the maximum impact load).

The maximum impact load on the grid in terms of the % change for each of the comparison study cases is presented in Table 1.

7. The loading tests performed on the assembly models of this study are much less severe (less displacement and stress response) than those expected to be encountered in typical seismic or LOCA events. Justify that damping values arrived at from the "low load" testing are relevant for response levels expected in limiting seismic and LOCA conditions.

Response

Damping from coolant flow is practically independent of amplitude, yet the structural damping (mainly due to rod frictions in the grid cells) increases with increasing amplitude, at least up to [b,c,d]. This [b,c,d] peak to peak amplitude corresponds to the approximate maximum possible fuel assembly deflection (cumulated gap in an assembly row). Hence, the use of damping values derived from low amplitude tests is conservative for high amplitude response expected in limiting seismic and LOCA conditions.

Table 1 Results of Damping Variation Study on Core Structural Model

b,c,d

b, c, d

Figure 1 Damping Measurement Under Axial Flow for Mode 1

b, c, d

Figure 2 Damping Measurement Under Axial Flow for Mode 2

b, c, d

Figure 3 Damping Measurement Under Axial Flow for Mode 3